

# Non-Hermitian and Zeno limit of quantum systems under rapid measurements

Felix Thiel <sup>\*</sup>

*Department of Physics, Institute of Nanotechnology and Advanced Materials, Bar-Ilan University, Ramat-Gan 52900, Israel  
and Physikalisches Institut, Albert-Ludwigs-Universität Freiburg, Hermann-Herder-Straße 3, 79104 Freiburg, Germany*

David A. Kessler 

*Department of Physics, Bar-Ilan University, Ramat-Gan 52900, Israel*



(Received 1 May 2020; accepted 11 June 2020; published 21 July 2020)

We investigate two models of a quantum system under rapid measurement performed to detect whether the system is in a given state  $|\psi_d\rangle$ . In the first, the detection process is modeled via an imaginary potential  $2i\hbar|\psi_d\rangle\langle\psi_d|/\tau$ . In the second approach, repeated strong projective measurements are performed on the otherwise unitarily evolving system with a fixed high frequency  $1/\tau$ . We compare the statistics of the random time  $T$  of first successful detection for the two models, considering both its probability density function  $F(t)$  and the moments  $\langle T^m \rangle$ . We show, by a direct comparison of the two solutions, that both approaches yield the same results for  $F(t)$  (and so the moments) in the small- $\tau$  limit, also called the Zeno limit, as long as the initial state  $|\psi_{in}\rangle$  is not parallel to the detection state, so that  $|\langle\psi_d|\psi_{in}\rangle| < 1$ . When this condition is violated, however, the low probability density to detect the state on timescales much larger than  $\tau$  is precisely a factor of 4 smaller in the non-Hermitian model. We express the solution of the Zeno limit of both problems formally in terms of an electrostatic analogy. Our results are corroborated by numerical simulations.

DOI: [10.1103/PhysRevA.102.012218](https://doi.org/10.1103/PhysRevA.102.012218)

## I. INTRODUCTION

Isolated quantum systems evolve unitarily according to the Schrödinger equation with a Hermitian Hamiltonian until a measurement, obeying the collapse postulate, is performed [1,2]. Recently, there has been increasing interest in repeatedly measured quantum systems [3–9], where the unitary evolution is disrupted periodically. In the quantum first-detection problem [10–29], a detector probes the system repeatedly as to whether or not it resides in a given target state  $|\psi_d\rangle$ . The quantity of interest is the (random) first-detection time  $T$ , the time of the first successful detection attempt.<sup>1</sup> This is a generalization of the time-of-arrival problem [30–39] and the quantum analog to the important first-passage problem of statistical mechanics [40–44]. In the context of quantum information, it can also be seen as a protocol for quantum search [10,45–50] or state transfer [51].

The detection protocol is the sequence of times  $\{t_1, t_2, t_3, \dots\}$  at which the observer attempts to detect the system. In the stroboscopic detection protocol, the system is probed every  $\tau$  time units,  $t_n = n\tau$ , and  $T$  can only assume an integer multiple of the detection period  $\tau$ . The detection protocol is a pragmatic way to resolve the problem with continuously observed quantum systems, i.e., the Zeno effect [52–57]. This latter describes the lockdown of quantum

evolution that occurs when the system is rapidly measured. In the Zeno limit, when  $\tau \rightarrow 0$  and the detection frequency diverges, the system dynamics appears frozen in comparison to the detection process. Therefore, the system cannot reach the detection space, making successful detection impossible. The first-detection probability then vanishes, an effect that has been called the quantum Zeno paradox.

The dynamics of this stroboscopic measurement protocol can be analyzed in terms of the nonunitary operator  $(1 - |\psi_d\rangle\langle\psi_d|)e^{-i\hat{H}\tau/\hbar}$ . The question then naturally arises of how this stroboscopic dynamics is related to the non-Hermitian Hamiltonian, or optical potential, which has been introduced to model the loss of probability due to quantum transitions or equivalently quantum traps [58,59]

$$\hat{H}_{\text{NH}} = \hat{H} - i\hbar\Gamma|\psi_d\rangle\langle\psi_d|. \quad (1)$$

The connection between these two problems was already proposed by Allcock [31], who showed in the context of a measurement of whether the particle is in the region  $x > 0$  that  $\Gamma = 2/\tau$  and that reducing  $\tau$  to increase temporal resolution leads to difficulties, later subsumed under the Zeno paradox rubric. This connection was later employed by Muga and co-workers, motivated the use of an optical potential by models where stimulated photon emission from the system signals its arrival [33,35–37,60]. Schulman showed that  $\Gamma = 2/\tau$  also in the case of a two-level system [61] and discussed the connection of the Zeno limit to continuous monitoring. Equation (1), which was studied intensively in Ref. [59], is important in its own right, because non-Hermitian terms appear when modeling the finite lifetime of certain energy states, when

<sup>\*</sup>thiel@posteo.de

<sup>1</sup>We use the capital letter to denote the first-detection time as a random variable, i.e.,  $T$ , and we use a lowercase letter  $t$  to denote its possible values as in the probability density function  $F(t)$ .

dealing with dissipative optical media, in quantum jump approaches, or in certain quantum transport models [59,62–74]. Non-Hermitian systems are also readily implemented experimentally [75–79]. It should be noted that the dissipation term in Eq. (1) can be derived from a system-bath coupling [80], but here our interest is in comparing and contrasting it to the stroboscopic measurement dynamics, particularly in the Zeno limit.

Our primary goal in this work is to use the recently obtained renewal equation solution to the stroboscopic dynamics problem to examine the connection to the solution of the time-independent Schrödinger equation with the non-Hermitian Hamiltonian (NHH) (1). One motivation for this is, given that the previous approaches use a perturbative approach to calculate the leading-order non-Hermitian Hamiltonian of the stroboscopic approach, one might be concerned about the presence of nontrivial effects at long times. Another is just to see exactly how the two solutions are related. We will show how to recover the identity of the two solutions in the Zeno limit, provided that the initial state is orthogonal to the detection state, in which case the dynamics is slow, with a timescale of order  $1/\tau$ . We then treat the case where the initial state is not orthogonal to the detection state. There, in the Zeno limit, there is an initial fast transient, over a timescale of order  $\tau$ , in the NHH case. For the stroboscopic dynamics, the transient consists of the first measurement only, which is also a time period of exactly  $\tau$ , after which the dynamics is slow. We then relate the post-transient dynamics of the two models and see that when the initial state is *parallel* to the detection state, the slow dynamics differs by a factor of 4 in the decay statistics. In Sec. V we exemplify these results through a number of specific models, namely, the nearest-neighbor length-6 ring and the infinite line, as well as a random Hamiltonian. We then proceed to discuss this limiting Zeno solution in more detail, relating it to the solution of a particular electrostatic problem. This electrostatic problem defines all the quantities necessary for constructing the limiting Zeno solution. Section VIII briefly discusses the behavior close to the return problem, i.e., for initial states that are almost parallel to  $|\psi_d\rangle$ . We close in Sec. IX with a discussion and summary. Some additional details are given in the Appendices. Appendix A presents the adiabatic elimination of the fast mode in Eq. (1) and Appendix B discusses the limit  $\tau \rightarrow \infty$  of very slow detectors for the non-Hermitian Schrödinger equation. Appendix C presents some details of the infinite line calculations. Finally, Appendix D explains how we obtained our numerical results.

## II. FORMAL SOLUTIONS TO BOTH PROBLEMS

### A. Non-Hermitian Schrödinger equation

We first review the solution of the continuous-time problem starting with the non-Hermitian Schrödinger equation (1), following closely the derivation in Ref. [59]. We denote the solution to Eq. (1) with initial condition  $|\psi(t=0)\rangle = |\psi_{\text{in}}\rangle$  by  $|\psi(t)\rangle$ . The squared norm of this state is the remaining probability in the system, the survival probability. Its negative derivative is the probability density function (PDF) of detec-

tion or dissipation times that equals

$$\begin{aligned} F^\Psi(t) &= -\frac{d}{dt} \langle \psi(t) | \psi(t) \rangle \\ &= -\left( \frac{d}{dt} \langle \psi(t) | \right) |\psi(t)\rangle - \langle \psi(t) | \frac{d}{dt} |\psi(t)\rangle \\ &= -\langle \psi(t) | \left[ \frac{i}{\hbar} \hat{H} - \frac{i}{\hbar} \hat{H} - 2\Gamma |\psi_d\rangle \langle \psi_d| \right] \psi(t) \\ &= 2\Gamma |\langle \psi_d | \psi(t) \rangle|^2 =: 2\Gamma |\Psi(t)|^2, \end{aligned} \quad (2)$$

where we introduced the overlap of the solution with the detection state  $\Psi(t) := \langle \psi_d | \psi(t) \rangle$ , which is the only piece of  $|\psi(t)\rangle$  that we actually need. Hereafter  $\Psi(t)$  is called the wave function. We append a sub- or superscript  $\Psi$  to quantities derived from the NHH framework. We apply a Laplace transform to Eq. (2), for which we use the Laplace partners  $\Psi(s) := \int_0^\infty dt e^{-st} \Psi(t)$  and  $\Psi(t) = \int_{\mathcal{B}} ds e^{st} \Psi(s) / 2\pi i$ :<sup>2</sup>

$$F^\Psi(s) := \int_0^\infty dt e^{-st} F^\Psi(t) = 2\Gamma \int_{\mathcal{B}} \frac{d\sigma}{2\pi i} \Psi^*(s - \sigma) \Psi(\sigma). \quad (3)$$

Here  $f^*(z) := [f(z^*)]^*$  and  $z^*$  is the complex conjugate. The integration contour is the Bromwich path  $\mathcal{B} := \{0^+ + i\omega \mid \omega \in \mathbb{R}\}$  that lies directly to the right of the imaginary axis. To obtain Eq. (3) we used that  $[\Psi(t)]^*$  transforms to  $\Psi^*(s)$  and that products in the time domain become convolutions in the Laplace domain. Furthermore, we have  $\text{Re}(s) > \text{Re}(\sigma) \geq 0$ . It is important to note that the complex contour integral in Eq. (3) picks up only the residues of  $\Psi(\sigma)$ , but not those of  $\Psi^*(s - \sigma)$ .

In addition to the PDF of  $T$ , we are also interested in the total detection probability  $P_{\text{det}}$  and in  $T$ 's (conditional) moments:

$$P_{\text{det}} := \int_0^\infty dt F(t), \quad \langle T^m \rangle := \frac{1}{P_{\text{det}}} \int_0^\infty dt t^m F(t). \quad (4)$$

Here  $P_{\text{det}}$  is the fraction of experimental runs in which the detector finds something at all. It is also the normalization of the first-detection time PDF. In addition,  $\langle T^m \rangle$  is the  $m$ th moment of  $T$  provided that the system was detected at all. Obviously, Eq. (4) holds for the stroboscopic framework as well, whence the lack of superscripts.

Instead of computing these quantities in the time domain, we can also obtain them from the Laplace quantity  $\Psi(s)$ , by using a version of Parseval's theorem

$$P_{\text{det}}^\Psi = 2\Gamma \int_{\mathcal{B}} \frac{ds}{2\pi i} \Psi^*(-s) \Psi(s), \quad (5)$$

$$\langle T^m \rangle^\Psi = \frac{2\Gamma}{P_{\text{det}}^\Psi} \int_{\mathcal{B}} \frac{ds}{2\pi i} \Psi^*(-s) \left( -\frac{d}{ds} \right)^m \Psi(s). \quad (6)$$

Here we have expressed the integral as a Laplace transform at  $s = 0^+$  and proceeded by using  $tf(t) \mapsto -\frac{d}{ds} f(s)$ . Let us now determine  $\Psi(s)$ .

<sup>2</sup>We use the same symbol for functions in the original and image domains. In our convention, the functions are identified by their arguments.

To do so, we apply a Laplace transform to Eq. (1). Here we explicitly use the initial condition  $|\psi_{\text{in}}\rangle$ , because  $(d/dt)f(t) \mapsto sf(s) - f(t=0)$ . We write  $|\psi(s)\rangle := \int_0^\infty dt e^{-st} |\psi(t)\rangle$ ,

$$i\hbar[s|\psi(s)\rangle - |\psi_{\text{in}}\rangle] = \hat{H}|\psi(s)\rangle - i\Gamma\hbar|\psi_{\text{d}}\rangle\langle\psi_{\text{d}}|\psi(s)\rangle. \quad (7)$$

The equation is rearranged

$$|\psi(s)\rangle = \left[ s + \frac{i}{\hbar}\hat{H} \right]^{-1} [|\psi_{\text{in}}\rangle - \Gamma|\psi_{\text{d}}\rangle\langle\psi_{\text{d}}|\psi(s)\rangle], \quad (8)$$

multiplied by  $\langle\psi_{\text{d}}|$  from the left, and solved for  $\langle\psi_{\text{d}}|\psi(s)\rangle = \Psi(s)$ ,

$$\Psi(s) = \frac{\langle\psi_{\text{d}}|\frac{1}{s+\frac{i}{\hbar}\hat{H}}|\psi_{\text{in}}\rangle}{1 + \Gamma\langle\psi_{\text{d}}|\frac{1}{s+\frac{i}{\hbar}\hat{H}}|\psi_{\text{d}}\rangle} =: \frac{v_\Psi(s)}{1 + \Gamma u_\Psi(s)}, \quad (9)$$

where we have abbreviated

$$u_\Psi(s) := \langle\psi_{\text{d}}|\frac{1}{s+\frac{i}{\hbar}\hat{H}}|\psi_{\text{d}}\rangle, \quad v_\Psi(s) := \langle\psi_{\text{d}}|\frac{1}{s+\frac{i}{\hbar}\hat{H}}|\psi_{\text{in}}\rangle. \quad (10)$$

Thus  $u_\Psi(s)$  and  $v_\Psi(s)$  are, respectively, the diagonal and off-diagonal matrix elements of the Hamiltonian's resolvent. In the return problem, when the initial and detection states are identical,  $v_\Psi(s) = u_\Psi(s)$ , but for the transition problem, where these two states are different, the two quantities are likewise different. Thus, specification of the Hamiltonian, together with the initial and detection states, yields the two functions  $u_\Psi(s)$  and  $v_\Psi(s)$ . From these one finds, via Eq. (9),  $\Psi(s)$ , which in turn gives the PDF  $F^\Psi(s)$  and all moments via integration.

### B. Stroboscopic detection protocol

We now review the solution of the stroboscopic detection protocol. Here the detection time can only assume integer multiples of  $\tau$ . Consequently, the (quasi-continuous-time) PDF of  $T$  must be a comb of  $\delta$  functions, that is,  $F^\Psi(t) = \sum_{n=1}^\infty |\varphi_n|^2 \delta(t - n\tau)$ . The first-detection amplitude's squared modulus  $|\varphi_n|^2$  gives the probability that the  $n$ th detection attempt is the first successful one. Here  $\varphi_n$  is given by [18,24]

$$\varphi_n = \langle\psi_{\text{d}}|\hat{U}(\tau)[(1 - \hat{D})\hat{U}(\tau)]^{n-1}|\psi_{\text{in}}\rangle, \quad (11)$$

where  $\hat{D} = |\psi_{\text{d}}\rangle\langle\psi_{\text{d}}|$  is the detection projector and  $\hat{U}(\tau) := e^{-i\tau\hat{H}/\hbar}$  is the evolution operator. According to [24], it can alternatively be obtained from a renewal equation via

$$\varphi_n = \langle\psi_{\text{d}}|[\hat{U}(\tau)]^n|\psi_{\text{in}}\rangle - \sum_{m=1}^{n-1} \langle\psi_{\text{d}}|[\hat{U}(\tau)]^m|\psi_{\text{d}}\rangle\varphi_{n-m}. \quad (12)$$

The generating function  $\varphi(z) := \sum_{n=1}^\infty \varphi_n z^n$  can be obtained from this equation by multiplying it by  $z^n$  and then summing over all  $n$  from one to infinity. This recovers the definition of  $\varphi(z)$  on the left-hand side. The convolution on the right-hand side becomes a product in the  $z$  domain, the terms  $[\hat{U}(\tau)]^n$  are gathered in a geometric series, and the equation is solved for  $\varphi(z)$  [24]:

$$\varphi(z) = \frac{\langle\psi_{\text{d}}|\frac{z\hat{U}(\tau)}{1-z\hat{U}(\tau)}|\psi_{\text{in}}\rangle}{\langle\psi_{\text{d}}|\frac{1}{1-z\hat{U}(\tau)}|\psi_{\text{d}}\rangle} =: \frac{v_\varphi(z) - \langle\psi_{\text{d}}|\psi_{\text{in}}\rangle}{u_\varphi(z)}. \quad (13)$$

Analogously to Eq. (9), we have defined

$$u_\varphi(z) := \langle\psi_{\text{d}}|\frac{1}{1-z\hat{U}(\tau)}|\psi_{\text{d}}\rangle, \quad v_\varphi(z) := \langle\psi_{\text{d}}|\frac{1}{1-z\hat{U}(\tau)}|\psi_{\text{in}}\rangle. \quad (14)$$

Here  $u_\varphi(z)$  is the (slightly differently defined) resolvent of the evolution operator and  $v_\varphi(z)$  is equal to  $u_\varphi(z)$  in the return problem. The sub- or superscript  $\varphi$  denotes quantities derived from the stroboscopic detection protocol.

This generating function reappears in the Laplace transform  $F^\varphi(s)$ , which is the generating function of the product  $\varphi_n^* \varphi_n$  evaluated at  $z = e^{-s\tau}$ . Again using that products in the time domain become convolutions in the  $z$  domain, we find

$$F^\varphi(s) = \sum_{n=1}^\infty \varphi_n^* \varphi_n e^{-ns\tau} = \oint_{\mathcal{C}} \frac{dz}{2\pi iz} \varphi^* \left( \frac{e^{-s\tau}}{z} \right) \varphi(z), \quad (15)$$

a result analogous to Eq. (3). Here the integration follows the Cauchy contour  $\mathcal{C} = \{e^{i\omega+0^-} \mid \omega \in [-\pi, \pi]\}$  just inside the unit circle. To compute the total detection probability and the moments, we use  $n f_n \mapsto z \frac{d}{dz} f(z)$  and find

$$P_{\text{det}}^\varphi = \oint_{\mathcal{C}} \frac{dz}{2\pi iz} \varphi^* \left( \frac{1}{z} \right) \varphi(z), \quad (16)$$

$$\langle T^m \rangle^\varphi = \frac{1}{P_{\text{det}}^\varphi} \oint_{\mathcal{C}} \frac{dz}{2\pi iz} \varphi^* \left( \frac{1}{z} \right) \left( z \frac{d}{dz} \right)^m \varphi(z). \quad (17)$$

Knowledge of the generating function  $\varphi(z)$  is sufficient to obtain all quantities pertaining to the stroboscopic detection protocol.

### III. SMALL- $\tau$ LIMIT OF THE STROBOSCOPIC DETECTION PROTOCOL

Starting from Eq. (15), we now demonstrate how (and under what conditions) the solution of the non-Hermitian Schrödinger equation  $F^\Psi(t)$  emerges from  $\varphi_n$  in the limit of small  $\tau$  and large  $n$  such that  $t = n\tau$  remains constant. The limit  $n \rightarrow \infty$  is most conveniently taken in the  $z$  domain, where it corresponds to  $|z| \rightarrow 1^-$ , i.e., approaching closer and closer to the unit circle.

The two key steps are the variable change  $z = e^{-s\tau}$  and the asymptotic equality

$$\frac{1}{1 - e^{-s\tau}} = \frac{1}{s\tau} + \frac{1}{2} + O(\tau), \quad (18)$$

which is used to expand

$$\begin{aligned} & \langle\psi|\frac{1}{1 - e^{-\tau(s+i\hat{H}/\hbar)}}|\psi'\rangle \\ &= \frac{1}{\tau} \langle\psi|\frac{1}{s + \frac{i}{\hbar}\hat{H}}|\psi'\rangle + \frac{\langle\psi|\psi'\rangle}{2} + O(\tau) \end{aligned} \quad (19)$$

for two arbitrary states  $|\psi\rangle$  and  $|\psi'\rangle$ . In terms of the previously defined functions, this means

$$u_\varphi(e^{-s\tau}) \sim \frac{1}{\tau} u_\Psi(s) + \frac{1}{2}, \quad (20)$$

$$v_\varphi(e^{-s\tau}) \sim \frac{1}{\tau} v_\Psi(s) + \frac{\langle\psi_{\text{d}}|\psi_{\text{in}}\rangle}{2}. \quad (21)$$

At this point, it is convenient to assume that the initial state has no overlap with the detection state  $\langle \psi_d | \psi_{\text{in}} \rangle = 0$ . We will in the next section deal with the more general problem. Plugging these results into the generating function  $\varphi(z = e^{-s\tau})$  gives us the relation

$$\varphi(e^{-s\tau}) \sim \frac{\frac{2}{\tau} \langle \psi_d | \frac{1}{s + \frac{i}{\hbar} \hat{H}} | \psi_{\text{in}} \rangle}{1 + \frac{2}{\tau} \langle \psi_d | \frac{1}{s + \frac{i}{\hbar} \hat{H}} | \psi_d \rangle} = \frac{2}{\tau} \Psi(s). \quad (22)$$

The result is, up to the factor  $2/\tau$ , just the wave function  $\Psi(s)$  of the NHH problem, with the identification  $\Gamma = 2/\tau$ . The Laplace-transformed wave function  $\Psi(s)$  appears in Eq. (15) after the change of variables  $z = e^{-\sigma\tau}$  with  $dz = -\tau z d\sigma$ . This changes the Cauchy contour to the proto-Bromwich path  $\mathcal{B}_\tau := \{0^+ + i\omega \mid \omega \in [-\pi/\tau, \pi/\tau]\}$ , which converges to the inverse Laplace transform's Bromwich path as  $\tau \rightarrow 0$ . One then finds

$$F^\varphi(s) \sim \frac{4}{\tau} \int_{\mathcal{B}_\tau} \frac{d\sigma}{2\pi i} \Psi^*(s - \sigma) \Psi(\sigma), \quad (23)$$

recovering Eq. (3) after the replacement (22). We have thus shown that  $F^\varphi(t) \sim F^\Psi(t)$ . Integration of this relation immediately yields  $\langle T^m \rangle^\varphi \sim \langle T^m \rangle^\Psi$  as well, so as expected the stroboscopic protocol does reduce to the NHH formalism in the Zeno limit  $\tau \ll 1$ , conditioned however on the orthogonality of the detection state to the initial state.

#### IV. SMALL- $\tau$ LIMIT FOR OVERLAPPING INITIAL AND DETECTION STATES

Before we turn to analyze the more general situation  $\langle \psi_{\text{in}} | \psi_d \rangle \neq 0$ , let us note that when the initial and detection states are orthogonal, the typical timescale on which  $F(t)$  decays is slow, that is,  $O(\Gamma) = O(1/\tau)$ . We will show this explicitly in Sec. VII. This somewhat nonintuitive result is a consequence of the quantum Zeno effect. The large magnitude  $\Gamma = 2/\tau$  of the optical potential on  $|\psi_d\rangle$  results in effective reflection of the wave function off the detection state. Thus the overlap of the wave function on the detection state  $\Psi(t) = \langle \psi_d | \psi(t) \rangle$  is always small of  $O(1/\Gamma^2) = O(\tau^2)$ , resulting in a slow  $O(1/\Gamma) = O(\tau)$  decay of probability.

This situation obviously cannot hold in the case when  $\langle \psi_d | \psi_{\text{in}} \rangle \neq 0$ , since the overlap initially is of order unity. What happens in this case is that the overlap rapidly decays to its typically small value over the short timescale  $O(\tau) = O(1/\Gamma)$ . Thus, in the small- $\tau$  limit, we can map the  $\langle \psi_d | \psi_{\text{in}} \rangle \neq 0$  case to an equivalent  $\langle \psi_d | \psi_{\text{in}} \rangle = 0$  case after this short transient.

Similarly, in the stroboscopic detection protocol, when  $\tau \ll 1$  and  $\langle \psi_d | \psi_{\text{in}} \rangle \neq 0$  there is an initial transient after which the problem reduces to that of an equivalent  $\langle \psi_d | \psi_{\text{in}} \rangle = 0$  case. The only difference from the NHH case is that the transient only lasts until the first-detection attempt, as opposed to decaying exponentially.

So, to proceed, we first analyze the NHH case by considering the survival probability after a very short time. Clearly, when  $\Gamma$  is very large and the initial state is equal to the detection state, most of the probability amplitude dissipates shortly after preparation. As we will demonstrate in detail below, the non-Hermitian Hamiltonian of Eq. (1) has exactly one

fast mode  $|\psi_f\rangle$  with eigenvalue  $-i\hbar\Gamma + \hbar\omega_0 + O(1/\Gamma)$ , where  $\omega_0 = \langle \psi_d | \hat{H} | \psi_d \rangle / \hbar$ . The fast mode is given to  $O(1/\Gamma)$  by

$$|\psi_f\rangle = \left[ \mathbb{1} + \frac{i}{\hbar\Gamma} (\mathbb{1} - \hat{D}) \hat{H} \right] |\psi_d\rangle. \quad (24)$$

Over short times  $1/\Gamma \ll t \ll 1$ , all of the wave function's overlap with the fast mode will be lost. In the case of partial but not complete overlap between initial and detection states  $0 < |\langle \psi_d | \psi_{\text{in}} \rangle|^2 < 1$ , the solution  $|\psi(t)\rangle$  of Eq. (1) at small times is given to leading order by

$$\begin{aligned} |\psi(t)\rangle &\sim e^{-t(\Gamma + i\omega_0)} |\psi_f\rangle \langle \psi_f | \psi_{\text{in}} \rangle + (\mathbb{1} - |\psi_f\rangle \langle \psi_f|) |\psi_{\text{in}} \rangle \\ &\sim (\mathbb{1} - \hat{D}) |\psi_{\text{in}} \rangle. \end{aligned} \quad (25)$$

Thus, after the fast transient dies away,  $|\psi_{\text{in}}^{\text{eff}}\rangle_\Psi = (\mathbb{1} - \hat{D}) |\psi_{\text{in}}\rangle$  and the survival probability is  $S_\Psi = 1 - |\langle \psi_d | \psi_{\text{in}} \rangle|^2$ .

The situation is different for full overlap  $|\langle \psi_d | \psi_{\text{in}} \rangle|^2 = 1$ . Here, almost all of the probability is depleted during the transient and the post-transient ‘‘initial’’ wave function is

$$|\psi_{\text{in}}^{\text{eff}}\rangle_\Psi = \frac{1}{i\hbar\Gamma} (\mathbb{1} - \hat{D}) \hat{H} |\psi_d\rangle, \quad (26)$$

whose magnitude gives the tiny survival probability  $S_\Psi$ ,

$$S_\Psi \approx \frac{1}{\hbar^2 \Gamma^2} \langle \psi_d | \hat{H} (\mathbb{1} - \hat{D}) \hat{H} | \psi_d \rangle =: \frac{1}{4} \frac{\tau^2}{\tau_Z^2}, \quad (27)$$

where we replaced  $\Gamma = 2/\tau$  and  $\tau_Z^2 := \hbar^2 / \langle \psi_d | \hat{H} (\mathbb{1} - \hat{D}) \hat{H} | \psi_d \rangle$  is the Zeno time [81].

We now turn to the stroboscopic detection protocol. For partial overlap, to leading order, the detection probability in the first-detection attempt is  $|\varphi_1|^2 = |\langle \psi_d | \psi_{\text{in}} \rangle|^2$  and the survival probability is  $S_\varphi = 1 - |\varphi_1|^2 = 1 - |\langle \psi_d | \psi_{\text{in}} \rangle|^2$ . This is just the post-transient survival probability of the NHH problem and so both problems map onto calculating the subsequent survival of the post-transient state  $(\mathbb{1} - \hat{D}) |\psi_{\text{in}}\rangle$ . As we have seen above, this survival probability is identical to leading order in the two problems; the two problems are thus seen to yield identical results also for partial overlap.

For complete overlap, however, things are very different. For the stroboscopic protocol, we have that the first-detection attempt is almost surely successful and the probability of survival is due to the small probability that was transferred to other states in the small time  $\tau$ . The wave function immediately after the first measurement is

$$|\psi_{\text{in}}^{\text{eff}}\rangle_\varphi = (\mathbb{1} - \hat{D}) e^{-i(\tau\hat{H}/\hbar)} |\psi_d\rangle \sim -i \frac{\tau}{\hbar} (\mathbb{1} - \hat{D}) \hat{H} |\psi_d\rangle \quad (28)$$

and the survival probability is then

$$S_\varphi \approx \frac{\tau^2}{\hbar^2} \|(\mathbb{1} - \hat{D}) \hat{H} |\psi_d\rangle\|^2 = \frac{\tau^2}{\tau_Z^2}. \quad (29)$$

Thus, while the form of the post-transient wave function (28) is the same as that for the NHH, Eq. (26), there is a factor of 2 difference, under the identification  $\Gamma = 2/\tau$ , along with a factor of 4 discrepancy between Eqs. (27) and (29). This difference stems from the quantitative difference in the transient dynamics of the return problem in the two models. It arises from the fact that the evolution under stroboscopic detection is unitary until time  $\tau$ , when the first projective measurement is applied, while the evolution under Eq. (1) is

dissipative from the very beginning such that less amplitude survives.

To relate the total detection probability of both formalisms for complete overlap, we write  $P_{\text{det}}^\varphi = \sum_{n=2}^{\infty} |\varphi_n|^2 + 1 - S_\varphi \sim 4[P_{\text{det}}^\Psi - (1 - S_\Psi)] + 1 - S_\varphi$ . Since the survival probabilities are  $O(\tau^2)$ , we can neglect them for  $P_{\text{det}}$ . For the moments, these initial discrepancies are not relevant. We find

$$P_{\text{det}}^\varphi \sim 4P_{\text{det}}^\Psi - 3, \quad \langle T^m \rangle^\varphi \sim \frac{4P_{\text{det}}^\Psi}{4P_{\text{det}}^\Psi - 3} \langle T^m \rangle^\Psi \quad (30)$$

for  $|\langle \psi_d | \psi_{\text{in}} \rangle| = 1$ . Any other initial condition gives  $P_{\text{det}}^\varphi \sim P_{\text{det}}^\Psi$  and  $\langle T^m \rangle^\varphi \sim \langle T^m \rangle^\Psi$ . We find from Eq. (30) that  $P_{\text{det}}^\varphi = 1 \Leftrightarrow P_{\text{det}}^\Psi = 1$ . Furthermore, the equivalence of the total detection probability must obviously break down when  $P_{\text{det}}^\Psi < 3/4$ , which defines a critical upper limit for  $\tau$ .

Note that the above expressions for the survival probabilities could be made coincident if  $\hbar/\tau$  is used as the optical potential strength in Eq. (1). Then, however, all remaining aspects of  $F^\Psi(t)$  are then not simply related to  $F^\varphi(t)$  as the following numerical investigations will show.

## V. EXAMPLES

We demonstrate our results in three models. The first is the tight-binding model on the benzene ring, i.e., a ring with six sites

$$\hat{H}_B := -\gamma \sum_{x=0}^5 [|x\rangle\langle x|x-1 + |x\rangle\langle x|x+1|], \quad (31)$$

with periodic boundary conditions such that  $|x+6\rangle = |x\rangle$ . Here  $\gamma$  is the hopping energy that determines the width of the spectrum. The Hamiltonian  $\hat{H}_B$  has four energy levels  $-2\gamma$ ,  $-\gamma$ ,  $\gamma$ , and  $2\gamma$ . The second system is a random  $(32 \times 32)$ -dimensional Hamiltonian  $\hat{H}_R$  taken from the Gaussian unitary ensemble. This Hamiltonian's lack of symmetries, its random energy levels, and eigenstates demonstrate that our results are not specific to any particular model. Nevertheless, we rescaled the spectrum of  $\hat{H}_R$  such that it lies between  $-2\gamma$  and  $2\gamma$ . This way, the timescales of both systems are comparable. For each of Figs. 1 and 3 one single sample matrix was used.<sup>3</sup> Finally, we also present a system with a continuous spectrum, the tight-binding model on the infinite line

$$\hat{H}_L := -\gamma \sum_{x=-\infty}^{\infty} [|x\rangle\langle x|x-1 + |x\rangle\langle x|x+1|], \quad (32)$$

whose spectrum again lies between  $-2\gamma$  and  $2\gamma$ , but is not discrete as before. The spectra of all three models lie in this range. The shortest timescale for all three Hamiltonians is thus given by the width of the energy spectrum:  $\hbar/4\gamma$ . All  $\tau$  values have to be compared to this shortest system timescale  $0.25\hbar/\gamma$ . Since all models' energy and timescales are comparable, we measure  $\tau$  and any other time in units of  $\hbar/\gamma$ , which is henceforth set to one,  $\hbar/\gamma = 1$ .

<sup>3</sup>For Fig. 3 convergence of the stroboscopic data can be problematic. Therefore, we chose our matrices from a subensemble of the Gaussian unitary ensemble for which this issue is not so severe (see Appendix D).

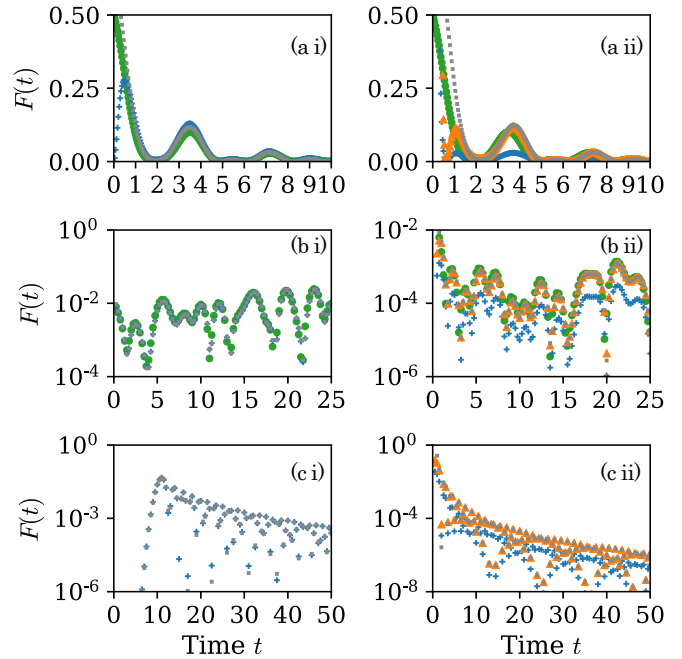


FIG. 1. Comparison of  $F^\varphi(t)$  (gray squares),  $F^\Psi(t)$  (blue pluses), the Zeno approximation [green circles, Eq. (68), not for (c)], and the corrected non-Hermitian approach with an additional factor of 4 [orange triangles, only (ii)] (a) for the benzene ring, (b) for the random Hamiltonian, and (c) on the infinite line. Detection is performed at the origin  $|\psi_d\rangle = |0\rangle$ . The detection period is given by (a) and (c)  $\tau = 0.5$  and (b)  $\tau = 0.25$ . The initial states are (i)  $|\psi_{\text{in}}^{B,R}\rangle$  and  $|\psi_{\text{in}}^L\rangle = |20\rangle$  and (ii)  $|\psi_d\rangle$ . For the benzene ring the data were interpolated between the times  $n\tau$  to better compare the area  $t \approx \tau$ . In the transition problem  $F^\Psi(t)$ ,  $F^\varphi(t)$ , and the Zeno approximation agree almost perfectly for  $t \gtrsim \tau$ , but differ for small times [see (a)]. In the return problem a factor of 4 must be introduced to  $F^\Psi(t)$  to match the stroboscopic data (orange triangles). This also holds for the complicated dynamics of the random Hamiltonian.

For the benzene ring and the infinite line, the detection state was chosen to be a position eigenstate. For the random Hamiltonian, we did the same in the sampled basis of the matrix such that

$$|\psi_d^{B,R,L}\rangle = |0\rangle. \quad (33)$$

We investigated a total of four initial states for the benzene ring:

$$\begin{aligned} |\psi_{\text{in}}^{B,1}\rangle &= |1\rangle, & |\psi_{\text{in}}^{B,2}\rangle &= |3\rangle, \\ |\psi_{\text{in}}^{B,3}\rangle &= \sum_{x=0}^5 \frac{|x\rangle}{\sqrt{6}}, & |\psi_{\text{in}}^{B,4}\rangle &= |0\rangle. \end{aligned} \quad (34)$$

The last one is the detection state; the first one does not yield a unit total detection probability. The third is an eigenstate of the Hamiltonian. For the random Hamiltonian, we explored two initial states

$$|\psi_{\text{in}}^{R,1}\rangle = |1\rangle, \quad |\psi_{\text{in}}^{R,2}\rangle = |0\rangle = |\psi_d\rangle, \quad (35)$$

so the second initial state yields the return problem. Different position eigenstates have been chosen as initial states for the infinite line.

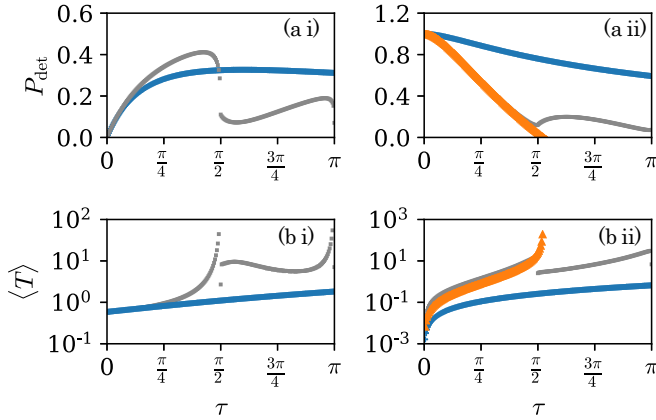


FIG. 2. (a) Total detection probability and (b) mean first-detection time for the infinite line model  $\hat{H}_L$ . The detection state is  $|\psi_d\rangle = |0\rangle$  and the initial state is (i)  $|1\rangle$  and (ii)  $|0\rangle$ . The stroboscopic data (gray squares), non-Hermitian data (blue pluses), and corrected non-Hermitian data (orange triangles, only for return problem) are shown. Singularities in the stroboscopic data are due to resonant detection periods. In the transition problem both approaches coincide for small  $\tau$ . For the return problem, the stroboscopic and corrected data coincide almost perfectly until  $\tau = \pi/2$ , where the corrected total detection probability also becomes negative.

Appendix D explains in detail how the numerical data were obtained. Throughout this article's figures, we stick to the following color code: Data for stroboscopic detection is given by gray squares, data from the non-Hermitian Schrödinger equation are depicted as blue pluses, corrected non-Hermitian data are given by orange triangles, and data from the Zeno approximation (discussed below) are depicted by green circles.

### A. Probability density functions

In Fig. 1 we start with plotting the PDFs  $F(t)$  of all three models. For the random Hamiltonian we take  $\tau = 0.25$  and for the others the relatively large value  $\tau = 0.5$ . We compare the data from the stroboscopic detection protocol with the solution of the non-Hermitian Schrödinger equation. (For the benzene Hamiltonian, the stroboscopic data are interpolated as explained in Appendix D.) Column (i) shows the transition problem where the initial and detection states are different. We see that both approaches lead to almost the same PDF, except in a boundary layer of size  $O(\tau)$  near  $t = 0$ . For these small times, the equivalence between both approaches loses its validity. Column (ii) shows the data for the return problem. Here the non-Hermitian data are off by a factor of 4, just as described in the preceding section. When this correction factor of 4 is introduced (orange triangles), we again find a nice data collapse, except in a small boundary layer around the origin. The boundary layer vanishes as  $\tau$  goes to zero. These observations even hold for the comparably complicated dynamics of the random system and for the infinite line, where the spectrum is continuous.

### B. Normalization and moments

Let us now compare the moments of the distributions  $F^\Psi(t)$  and  $F^\varphi(t)$ . In Fig. 2 we plotted the total detection prob-

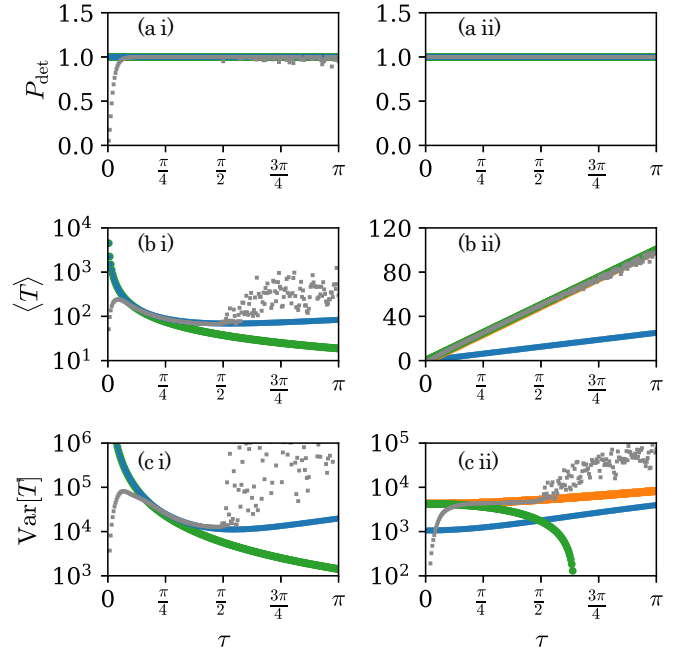


FIG. 3. First-detection statistics for the random Hamiltonian  $\hat{H}_R$ . The detection state is given by Eq. (33). The (a) total detection probability, (b) mean first-detection time, and (c) its variance are shown for the initial states given by Eq. (35). The stroboscopic data (gray squares), non-Hermitian data (blue pluses), corrected non-Hermitian data (orange triangles), and Zeno limit (green circles) are shown. Fluctuations in the stroboscopic data for  $\tau > \pi/2$  correspond to resonant detection times, which cannot be mapped to the non-Hermitian picture. The dip in the stroboscopic data for  $\tau \rightarrow 0$  is a numerical artifact due to slow convergence (see Appendix D). For small  $\tau$  all approaches give the same result. All approaches give the correct total detection probability (a), except for the resonant detection periods. In the transition problem (i), the non-Hermitian approach gives good results roughly until the first resonance. In the return problem (ii), the corrected non-Hermitian data or the Zeno approximation is more appropriate. The latter two describe the mean perfectly for almost all  $\tau$  (b ii). The non-Hermitian approach describes the variance better for intermediate  $\tau$  than the Zeno approximation (c ii).

ability [row (a)] and the mean first-detection time [row (b)] for the infinite line. (Higher moments do not exist, due to the power-law decay of the PDF [25].) Column (i) shows data for the initial state  $|\psi_{in}\rangle = |1\rangle$ , where the non-Hermitian and the stroboscopic data clearly only coincide for small  $\tau$ . Column (ii), on the other hand, depicts the return problem, when  $|\psi_{in}\rangle = |\psi_d\rangle = |0\rangle$ . Here the pure non-Hermitian data and the stroboscopic data only share its value at  $\tau = 0$ . The corrected result of Eq. (30), however, fits almost perfectly until  $\tau_{3/4} \approx \pi/2$ . This is a pleasant surprise. In fact, as we show in the Appendices, the difference between  $P_{det}^\Psi(\psi_d)$  and  $P_{det}^\varphi(\psi_d)$  is  $O(\tau^6)$  and so is tiny for small  $\tau$ . It is clear that the two results must diverge from each other beyond  $\tau_{3/4}$ , where  $P_{det}^\Psi(\tau_{3/4}) = 3/4$ , and thus  $4P_{det}^\Psi(\tau_{3/4}) - 3 = 0$ , i.e., when the corrected expression (30) becomes negative and thus non-physical.

The value  $\tau_c = \pi/2$  is also a special resonant value for the infinite line model [24,25]. Starting from this value, the Hamiltonian's spectrum stretched by a factor  $\tau$  does not “fit

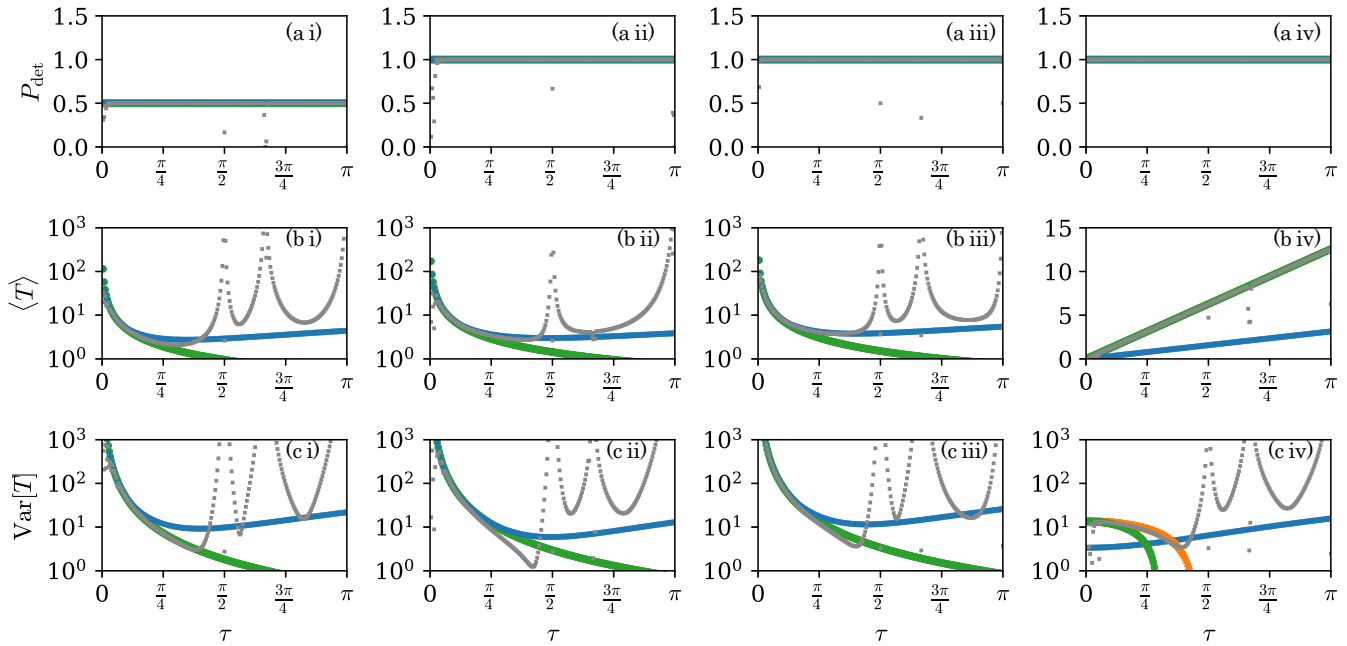


FIG. 4. First-detection statistics for the benzene ring  $\hat{H}_B$  [Eq. (31)]. The detection state is given by Eq. (33) and initial states are given by Eq. (34). The notation is as in Fig. 3 and the same conclusions hold here. Just like in that figure, the correction becomes necessary in the return problem (iv) and describes the stroboscopic data in a larger  $\tau$  range than the Zeno approximation (c iv). The divergences and dips in the stroboscopic data are due to resonant detection periods.

around the unit circle” anymore. Then the spectrum of  $\hat{H}$  and  $\hat{U}(\tau) = e^{-i\tau\hat{H}/\hbar}$  start to become fundamentally different, because eigenstates of the Hamiltonian around the band edges become dynamically equivalent. This aliasing effect has no counterpart in the non-Hermitian system. Still, we find an almost perfect data collapse between the stroboscopic data and the corrected non-Hermitian data of Eq. (30) for  $\tau < \tau_c$  in Fig. 2.

Systems with discrete energy spectra also feature critical detection periods, which are defined by the resonance condition  $(E_l - E_{l'})\tau = 0 \bmod 2\pi\hbar$ , when two energy levels become equivalent in  $\hat{U}(\tau)$ . In these systems, there is no  $\tau$  dependence in  $P_{\text{det}}$  [28], except at these exceptional values. The correction (30) to  $P_{\text{det}}^\Psi$  becomes meaningless, because the return problem yields  $1 = P_{\text{det}}^\varphi = P_{\text{det}}^\Psi$ , which results in  $4P_{\text{det}}^\Psi - 3 = 1$  as well. However, the correction factor is still important for the moments, as Figs. 3 and 4 show for the random Hamiltonian and the benzene ring, respectively. Both figures demonstrate how the non-Hermitian approach correctly predicts the total detection probability except at resonant detection periods, a hardly surprising exception. Higher moments of the stroboscopic detection protocol are well described by the non-Hermitian approach roughly until the first resonance, when both curves depart from each other. By virtue of our normalization of each system’s energy spectrum, this first resonance lies at  $\tau_c = \pi/2$ . We also see that the non-Hermitian data are not appropriate in the return problem, where the correction (30) must be used. This is particularly apparent in the return problem’s mean first-detection time  $M$ , which was shown to be quantized in Ref. [15]. There we have  $\langle T \rangle^\varphi = w\tau$  (discussed below), but  $\langle T \rangle^\Psi = w\tau/4$ . Introducing the correction factor of 4 makes the curves for the mean collapse for almost all  $\tau$ .

As we have demonstrated numerically, the non-Hermitian and the stroboscopic approach give equivalent results for small detection periods. In the return problem, however, the results coincide only after adjustment.

In general, they only coincide (after adjustment, in the case of the return problem) up to a relative error of  $O(\tau^2)$ . From this point of view, the good numerical correspondence is rather surprising.

## VI. DISCRETE ENERGY SPECTRA AND THE ELECTROSTATIC FORMALISM

From the perspective of the equivalence between  $F^\varphi(t)$  and  $F^\Psi(t)$ , one is still left with finding the distribution  $F^\Psi(t)$ , which poses a considerable problem for a general system. More tractable is the question of the actual small- $\tau$  limit of both systems. This question will be answered in Sec. VII for finite-dimensional systems with a discrete energy spectrum. As a first step, we will derive some general features that all finite-dimensional systems have in common. This will reveal the special nature of the return problem and help us to take the Zeno limit in the next section.

In this section we focus on systems with discrete energy spectra. These systems admit the usual diagonal form of the Hamiltonian

$$\hat{H} = \sum_l E_l \hat{P}_l = \sum_l E_l \sum_{m=1}^{g_l} |E_{l,m}\rangle \langle E_{l,m}|, \quad (36)$$

where  $E_l$  are the energy levels, each of them  $g_l$ -fold degenerate with eigenstates  $|E_{l,m}\rangle$  and eigenspace projector  $\hat{P}_l$ . Since we explicitly account for the degeneracies from the start, all energy levels are distinct  $E_l \neq E_{l'}$ .

We first consider the stroboscopic detection protocol and briefly review the results originally reported in Ref. [15]. Later we apply the same results to the non-Hermitian setup.

### A. Stroboscopic detection protocol

#### 1. Formal solution for the PDF

Using the diagonal form (36) in the definitions of Eq. (14) yields

$$u_\varphi(z) = \sum_{l=1}^w \frac{p_l}{1 - ze^{-i\tau E_l/\hbar}}, \quad v_\varphi(z) = \sum_{l=1}^w \frac{p_l q_l}{1 - ze^{-i\tau E_l/\hbar}}, \quad (37)$$

where  $p_l := \langle \psi_d | \hat{P}_l | \psi_d \rangle$  and  $p_l q_l := \langle \psi_d | \hat{P}_l | \psi_{in} \rangle$ . It should be noted that not all energy levels  $E_l$  actually contribute to the problem. Any energy level which has no overlap with the detection state, i.e., for which  $\hat{P}_l | \psi_d \rangle = 0$ , will not appear in either  $u_\varphi(z)$  or  $v_\varphi(z)$ . They can safely be ignored. Further,  $\hat{H}$  could even possess a continuous part of the spectrum, as long as it has no overlap with the detection state. This is what we mean when we talk about systems with a discrete spectrum.<sup>4</sup> We assume that  $w$  different energy levels appear in  $u_\varphi(z)$  and that for each of those  $p_l > 0$ . Naturally, we have  $\sum_{l=1}^w p_l = \langle \psi_d | \psi_d \rangle = 1$ , so none of them can be larger than unity. A similar normalization holds for the  $q_l$ , namely,  $\sum_{l=1}^w p_l q_l = \langle \psi_d | \psi_{in} \rangle$ . Apart from that, the  $q_l$  can be arbitrary complex numbers. Another implicit assumption in Eq. (37) is that resonant  $\tau$  are avoided such that all phase factors  $e^{-i\tau E_l/\hbar}$  are unique and no pair of terms yields the same denominator. Otherwise,  $w$  would need to be redefined.

The points  $z = e^{i\tau E_l/\hbar}$  are simple poles of the functions  $u_\varphi(z)$  and  $v_\varphi(z)$ . Nevertheless, these poles cancel in  $\varphi(z)$ , which is analytic in the unit disk. Still  $\varphi(z)$  has  $w - 1$  poles  $\mathfrak{z}_l$  outside the unit disk defined by

$$0 = u_\varphi(\mathfrak{z}_l). \quad (38)$$

These simple poles are crucial to writing down a formal solution to  $\varphi_n$ . This is achieved by a partial fraction decomposition of  $\varphi(z)$ . Note that when some rational function  $h(z) = f(z)/g(z)$  has the simple poles  $\mathfrak{z}_l$  [which are simple zeros of  $g(z)$ ] it admits the decomposition  $h(z) = \sum_l \frac{C_l}{z - \mathfrak{z}_l}$  and the coefficients can be obtained via Heaviside's formula

$$C_l = \lim_{z \rightarrow \mathfrak{z}_l} (z - \mathfrak{z}_l) h(z) = \frac{f(\mathfrak{z}_l)}{g'(\mathfrak{z}_l)}. \quad (39)$$

Applying this formula to  $\varphi(z)/z$  with Eq. (13) (so that  $g(z) = u_\varphi(z)$  and  $f(z) = [v_\varphi(z) - \langle \psi_d | \psi_{in} \rangle]/z$ ) gives

$$\varphi(z) = - \sum_{l=1}^{w-1} \frac{v_\varphi(\mathfrak{z}_l) - \langle \psi_d | \psi_{in} \rangle}{\mathfrak{z}_l u'_\varphi(\mathfrak{z}_l)} \frac{z}{1 - \frac{z}{\mathfrak{z}_l}}. \quad (40)$$

Expanding each geometric series gives  $\varphi_n$ :

$$\varphi_n = - \sum_{l=1}^{w-1} \frac{v_\varphi(\mathfrak{z}_l) - \langle \psi_d | \psi_{in} \rangle}{u'_\varphi(\mathfrak{z}_l)} \mathfrak{z}_l^{-n-1}. \quad (41)$$

<sup>4</sup>Mathematically speaking, our truncation or construction of  $\hat{H}$  ensures that  $|\psi_d\rangle$  is a cyclic vector of  $\hat{H}$  and that the space of vectors  $\{|\psi_d\rangle, \hat{H}|\psi_d\rangle, \hat{H}^2|\psi_d\rangle, \dots\}$  has dimension  $w$ .

Hence, knowledge about the poles  $\mathfrak{z}_l$  of  $\varphi(z)$  results in a decomposition of the detection amplitudes in terms of exponentially decaying modes. (They decay rather than grow because  $|\mathfrak{z}_l| > 1$ .)

#### 2. Electrostatic analogy

The poles themselves can be found from a nice electrostatic analogy. The starting point is Eq. (38), which has a trivial solution  $\mathfrak{z} = \infty$ . When this is removed by multiplication by  $\mathfrak{z}$ , one arrives at

$$0 = \mathfrak{z} u_\varphi(\mathfrak{z}) = \sum_{l=1}^w \frac{p_l}{\frac{1}{\mathfrak{z}} - e^{-i\tau E_l/\hbar}}. \quad (42)$$

We now construct the two-dimensional (2D) electrostatic potential

$$V_\varphi(x, y) := \sum_{l=1}^w p_l \ln \sqrt{[x - \cos(\frac{\tau E_l}{\hbar})]^2 + [y + \sin(\frac{\tau E_l}{\hbar})]^2} \quad (43)$$

by placing 2D point charges of magnitude  $p_l$  on each eigenvalue eigenvalue  $e^{-i\tau E_l/\hbar}$  of  $\hat{U}(\tau)$  on the unit circle. [Here we use the canonical mapping between the real and the complex plane:  $\mathbb{R}^2 \ni (x, y) \leftrightarrow x + iy \in \mathbb{C}$ .] Then the points  $\mathfrak{z}_V = 1/\mathfrak{z} = x + iy$  are seen to be  $V_\varphi(x, y)$ 's stationary points, i.e., the points of vanishing gradient  $\nabla_{(x,y)} V_\varphi(x, y) = \mathbf{0}$ . These gradient equations are exactly the real and imaginary parts of Eq. (42).

In the return problem, we have  $v_\varphi(z) = u_\varphi(z)$  and there is a relation between the poles  $\mathfrak{z}$  and the zeros  $n$  of  $\varphi(z)$ , because there is a symmetry between the  $u_\varphi(z)$  and its conjugate  $u_\varphi^*(z)$ :

$$u_\varphi(z) = - \left[ u_\varphi^* \left( \frac{1}{z} \right) - 1 \right]. \quad (44)$$

(Recall that  $u_\varphi^*(z) = [u_\varphi(z^*)]^*$ .) Equation (44) is easily seen from the definition of  $u_\varphi(z)$  and the unitarity of  $\hat{U}(\tau)$ . So if  $\mathfrak{z}$  is a root of  $u_\varphi(\mathfrak{z}) = 0$  [and thus a pole of  $\varphi(z)$ ], then  $n = 1/\mathfrak{z}^*$  is a root of  $u_\varphi(n) - 1 = 0$  [and thus a zero of  $\varphi(z)$  for the return problem; see Eq. (13)]. These zeros  $n = \mathfrak{z}_V^*$  are the conjugated stationary points of the two-dimensional electrostatic potential  $V_\varphi(x, y)$ . The operation  $n = 1/\mathfrak{z}^*$  that connects the zeros and poles is a reflection about the unit circle. Note that  $\varphi(z)$  has an additional trivial zero at  $z = 0$ , because  $u_\varphi(0) = 1$ , which is not mapped by the electrostatic analogy. Furthermore, note that  $\varphi(z)$  for the transition problem has different zeros than these stationary points. These, however, are not as important to the first-detection statistics, because only the poles  $\mathfrak{z}$  determine the decay modes.

#### 3. Return problem

In the return problem, when  $|\psi_{in}\rangle = |\psi_d\rangle$  and  $v_\varphi(z) = u_\varphi(z)$ , the knowledge of the poles is sufficient to describe all first-detection statistics. The electrostatic potential can then be used to describe these statistics [82,83]. The symmetry relation (44) is a peculiarity of the return problem and implies that  $\varphi^*(1/z) = 1/\varphi(z)$  when  $|\psi_{in}\rangle = |\psi_d\rangle$ . It follows from

Eq. (16) that the return state is almost surely detectable:

$$P_{\text{det}}(\psi_d) = \oint_C \frac{dz}{2\pi iz} \frac{\varphi(z)}{\varphi(z)} = 1. \quad (45)$$

With the same identity, we find that the mean first-detection time is a contour integral over a logarithmic derivative:

$$\langle T \rangle^\varphi = \tau \oint_C \frac{dz}{2\pi i} \frac{d}{dz} \ln \varphi(z) = w\tau. \quad (46)$$

By virtue of the argument principle of complex analysis, the contour integral over a logarithmic derivative is equal to the number of the function's zeros minus the number of poles. This number is  $w$ . In addition,  $\varphi(z)$  has no poles inside the unit disk. There are  $w - 1$  zeros found from the stationary points of Eq. (43) and one trivial zero at  $z = 0$ , where  $u_\varphi(z = 0) = 1$ . Therefore, the mean first-detection time of the return problem in the stroboscopic detection protocol is quantized and equal to the number of energy levels that appear in  $|\psi_d\rangle$  [15,21,23]. Equations (45) and (46) are nicely demonstrated in Figs. 3(ii) and 4(iv), where the total detection probability and the mean show constant and linear behavior, respectively.

Analytically finding the zeros of  $u_\varphi(z)$  or the stationary points of  $V_\varphi(x, y)$  is in general equally hard and not possible outside of some perturbative limit. Nevertheless, the above arguments, which are known for the stroboscopic detection protocol [15], can be applied directly to the non-Hermitian Schrödinger equation. There we can gain additional insights.

## B. Non-Hermitian Schrödinger equation

### 1. Formal solution for the PDF

Again, we express the resolvents in terms of the overlaps  $p_l$  and  $q_l$  as well as with the energy levels  $E_l$ :

$$u_\psi(s) = \sum_{l=1}^w \frac{p_l}{s + i\frac{E_l}{\hbar}}, \quad v_\psi(s) = \sum_{l=1}^w \frac{p_l q_l}{s + i\frac{E_l}{\hbar}}. \quad (47)$$

As before,  $v_\psi(s)$  and  $u_\psi(s)$  have poles at  $-iE_l/\hbar$ , which cancel in  $\Psi(s)$ . Here  $\Psi(s)$  has  $w$  simple poles  $s_l$  in the left half plane defined by the equation

$$0 = 1 + \frac{2}{\tau} u_\psi(s_l). \quad (48)$$

Using these poles, we can write down a partial fraction decomposition of  $\Psi(s)$ :

$$\Psi(s) = \frac{\tau}{2} \sum_{l=1}^w \frac{v_\psi(s_l)}{u'_\psi(s_l)} \frac{1}{s - s_l}. \quad (49)$$

Using the residue theorem, the inverse Laplace transform is easily performed:

$$\Psi(t) = \frac{\tau}{2} \sum_{l=1}^w \frac{v_\psi(s_l)}{u'_\psi(s_l)} e^{t s_l}. \quad (50)$$

Since all poles lie in the left half plane such that  $\text{Re}[s_l] < 0$ , all exponentials are decaying. Note that Eq. (48) has  $w$  roots as opposed to Eq. (38).

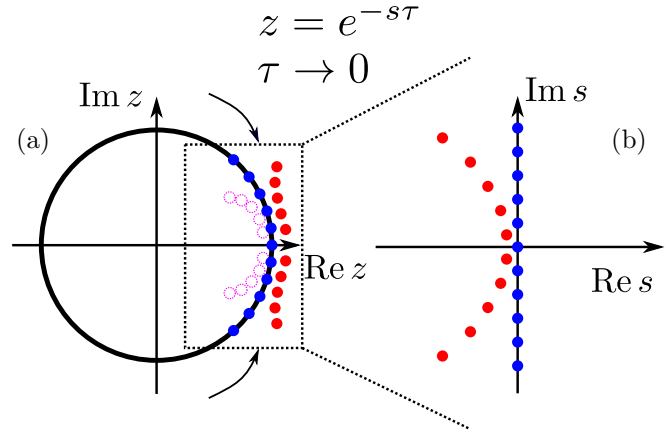


FIG. 5. Poles in the electrostatic analogy. (a) The eigenvalues  $e^{-iE_l\tau/\hbar}$  of  $\hat{U}(\tau)$  lie on the unit circle (blue closed circles). The poles  $\beta_l$  of  $\varphi(z)$  (red closed circles) lie outside the unit circle. Their mirror images  $\eta_l$  (magenta open circles) lie inside the unit disk. After equipping every one of  $\hat{U}(\tau)$ 's eigenvalues with an electric charge equal to the overlap  $p_l = \langle \psi_d | \hat{P}_l | \psi_d \rangle$ , Ref. [15] finds the mirrored poles as the stationary points of the electrostatic potential (43). As  $\tau$  decreases all points move to  $z = 1$  (arrows). (b) Our mapping  $z = e^{-s\tau}$  zooms in around  $z = 1$ . The unit circle's curvature is replaced by a constant force [see Eq. (51)]. The charges are placed at  $iE_l/\hbar$  on the imaginary axes. The poles  $s_l$  are the complex conjugates of the new electrostatic potential's stationary points.

### 2. Electrostatic analogy

Again, we can find an electrostatic analogy by inspecting Eq. (48). This time, the conjugated poles  $s^* = x + iy$  are given by the stationary points of the following electrostatic potential:

$$V_\psi(x, y) := \frac{\tau}{2} x + \sum_{l=1}^w p_l \ln \sqrt{x^2 + \left(y - \frac{E_l}{\hbar}\right)^2}. \quad (51)$$

Here a positive point charge of magnitude  $p_l$  is placed on each eigenvalue of the *Hamiltonian* on the imaginary axis. In contrast to the previous potential, there is an additional constant force proportional to  $\tau$ .

Recall from Sec. III that we related  $z$  and  $s$  via  $z = e^{-s\tau}$  and a subsequent small- $\tau$  expansion. The exponential maps the outside of the unit circle to the left half of a strip  $\{s \in \mathbb{C} \mid \text{Re}[s] < 0, |\text{Im}[s]| < \pi/\tau\}$ . Taking  $\tau \rightarrow 0$  enlarges this domain to the complete left half plane. During this procedure, the charges, which were originally on the unit circle, move to the imaginary axis. The curvature of the unit circle, which forced the zeros inside the unit disk, gets mapped to the constant-force term, which forces the poles into the left half plane. This ensures the boundedness of  $\Psi(t)$  (see also Fig. 5). Another way to relate Eqs. (38) and (48) is via Eq. (20), which reveals the latter as a straightforward small- $\tau$  version of the former. The advantage of  $V_\psi(x, y)$  over its counterpart  $V_\varphi(x, y)$  is the much easier geometry. All the charges lie on a line. This makes it possible to find all the poles in the Zeno limit, as will be presented in the next section.

Similar to the stroboscopic case, there is a relation between  $u_\Psi(s)$  and its conjugate:

$$-u_\Psi^*(-s) = u_\Psi(s). \quad (52)$$

Using this equation, one can relate the poles of  $\Psi(s)$  with those of  $\Psi^*(-s)$  in Eqs. (5) and (6).

Just as in the stroboscopic case, one finds a quantized mean first-detection time

$$\langle T \rangle^\Psi = \frac{w}{4} \tau \quad (53)$$

from complex function arguments. This is a result that will be explored in more depth elsewhere [29]. We did not find an equally nice analytical demonstration that  $P_{\text{det}}^\Psi(\psi_d) = 1$  for the non-Hermitian setup. This is however evident from our numerics in Figs. 3(a ii) and 4(a iv) and will be shown in the limit  $\tau \rightarrow 0$  in the next section. We also demonstrate it in the limit  $\tau \rightarrow \infty$  in Appendix B.

## VII. ZENO LIMIT IN THE ELECTROSTATIC FORMALISM

### A. Non-Hermitian Schrödinger equation

Starting with the electrostatic analogy, we can find all the poles when  $\tau$  is sufficiently small. Consider  $V_\Psi(x, y)$  from Eq. (51) first for vanishing  $\tau$ . Since all charges have the same sign and there is no constant force, the stationary points must lie on the imaginary axis, i.e.,  $x = 0$ , one between each pair of adjacent energies. Assume that the  $w$  energy levels are ordered, i.e.,  $E_l < E_{l+1}$ . We will then find one stationary point of  $V_\Psi(x, y)$  at  $0 + i\omega_l$  with  $E_l < \hbar\omega_l < E_{l+1}$ . We call the  $\omega_l$  the absorption frequencies. They are found by solving the equation

$$0 = -\frac{i}{\hbar} u_\Psi(-i\omega_l) = \langle \psi_d | \frac{1}{\hbar\omega_l - \hat{H}} | \psi_d \rangle, \quad (54)$$

i.e., they are the zeros of the resolvent. We plotted the resolvent for the benzene ring in Fig. 6, where it is apparent that the resolvent is a monotonic function between two energy values. Therefore, although the absorption frequencies are only defined implicitly, they are easy to find in practice. They interlace with the energy levels and are thus bracketed and the defining function is monotonic. Any numerical root finding algorithm will find them with ease. There are  $w - 1$  solutions  $\omega_l$ ,  $l = 1, \dots, w - 1$ , to Eq. (54). A similar interlacing for absorption and relaxation rates has been found for the first-passage problem of classical random walks [44].

Now we consider  $\tau > 0$  but small. The additional small constant force will shift the stationary points from  $i\omega_l$  slightly into the left half plane. Thus we make the following ansatz for the pole

$$s_l \sim -\lambda_l \tau - i\omega_l \quad (55)$$

and plug it into Eq. (48) together with Eq. (47), which yields

$$\begin{aligned} 0 &= \frac{\tau}{2} + \sum_{l'=1}^w \frac{p_{l'}}{-\lambda_{l'} \tau + \frac{i}{\hbar}(E_{l'} - \hbar\omega_{l'})} \\ &= \frac{\tau}{2} - \sum_{l'=1}^w \frac{p_{l'} [\lambda_{l'} \tau + \frac{i}{\hbar}(E_{l'} - \hbar\omega_{l'})]}{\lambda_{l'}^2 \tau^2 + \frac{1}{\hbar^2}(E_{l'} - \hbar\omega_{l'})^2} \end{aligned}$$

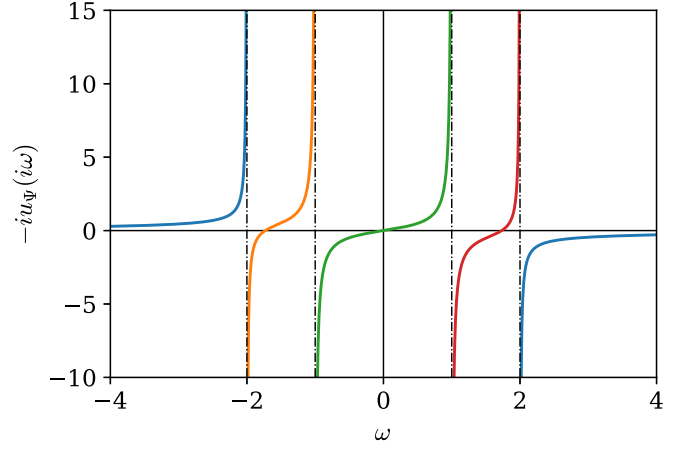


FIG. 6. Resolvent  $u_\Psi(s)$  for the benzene ring  $\hat{H}_B$ . We show  $\omega \mapsto -iu_\Psi(i\omega)$ . The dash-dotted lines, where  $u_\Psi(s)$  diverges, show the negative energy levels. The zeros of this function are the negative absorption frequencies  $-\omega_l$ . The derivative of  $u_\Psi(s)$  at these points is related to the absorption rates  $\lambda_l \tau$ . Clearly, one zero is located between two adjacent energy levels, and the function is monotonic in this interval as well. Therefore, the absorption frequencies are easily found numerically.

$$\begin{aligned} &\sim \frac{\tau}{2} - \sum_{l'=1}^w \frac{p_{l'} [\lambda_{l'} \tau + \frac{i}{\hbar}(E_{l'} - \hbar\omega_{l'})]}{\frac{1}{\hbar^2}(E_{l'} - \hbar\omega_{l'})^2} \\ &= \tau \left\{ \frac{1}{2} - \hbar^2 \lambda_l \sum_{l'=1}^w \frac{p_{l'}}{(E_{l'} - \hbar\omega_{l'})^2} \right\} - i\hbar \sum_{l'=1}^w \frac{p_{l'}}{E_{l'} - \hbar\omega_{l'}}. \end{aligned} \quad (56)$$

Higher-order terms in  $\tau$  were neglected to obtain the third line. Equating the imaginary part of the last line with zero results in Eq. (54), which shows that the imaginary part was correctly chosen. The absorption rate  $\lambda_l$  is determined from the last line's real part:

$$\lambda_l = \left[ 2\hbar^2 \sum_{l'=1}^w \frac{p_{l'}}{(E_{l'} - \hbar\omega_{l'})^2} \right]^{-1} = \frac{1}{2u'_\Psi(-i\omega_l)}. \quad (57)$$

This gives the missing part to Eq. (55) that determines the poles  $s_l$  for  $l = 1, \dots, w - 1$ . In addition to the poles, we need  $u'_\Psi(s)$  and  $v_\Psi(s)$  for Eq. (50). The first is determined by  $\lambda_l$  to leading order:

$$u'_\Psi(s_l) \sim u'_\Psi(-i\omega_l) = \frac{1}{2\lambda_l}, \quad l = 1, \dots, w - 1. \quad (58)$$

Furthermore, we find  $v_\Psi(s_l)$  in leading order. For the return problem, this is equal to  $v_\Psi(s_l) = u_\Psi(s_l) = -\tau/2$ . In the transition problem, we obtain

$$v_\Psi(s_l) \sim \langle \psi_d | \frac{1}{\frac{i}{\hbar}\hat{H} - i\omega_l} | \psi_{\text{in}} \rangle =: -i\theta_l, \quad (59)$$

which defines the transition times  $\theta_l$ .

We have thus found  $w - 1$  poles close to the imaginary axis. These determine the slow dynamics in  $\Psi(t)$ . However, Eq. (48) admits another pole far in the left half plane, which describes the fast dynamics of  $\Psi(t)$ . This pole is given in

leading order by

$$s_0 \sim -2/\tau - i\omega_0, \quad (60)$$

where  $\hbar\omega_0 = \langle \psi_d | \hat{H} | \psi_d \rangle$  is the mean energy of the detection state. For the derivative  $u'_\Psi(s_0)$  and for  $v_\Psi(s_0)$  we find

$$u'_\Psi(s_0) \sim -\frac{\tau^2}{4}, \quad v_\Psi(s_0) \sim -\frac{\tau}{2} \langle \psi_d | \psi_{in} \rangle. \quad (61)$$

Now we have gathered all the necessary ingredients to write down  $\Psi(t)$ . Using all the just derived results in Eq. (50), we arrive at

$$\Psi(t) \sim \begin{cases} \langle \psi_d | \psi_{in} \rangle e^{-t(2/\tau + i\omega_0)} - i\tau \sum_{l=1}^{w-1} \lambda_l \theta_l e^{-t(\lambda_l \tau + i\omega_l)} \\ e^{-t(2/\tau + i\omega_0)} - \frac{\tau^2}{2} \sum_{l=1}^{w-1} \lambda_l e^{-t(\lambda_l \tau + i\omega_l)} \end{cases}. \quad (62)$$

Here the first line corresponds to the transition problem and the second line corresponds to the return problem. Note that the fast dynamics is the same in both situations. The slow dynamics, however, is of different order in  $\tau$ .

Squaring the wave function and multiplying it by  $4/\tau$  gives the PDF  $F^\Psi(t)$ . We have, to leading order in  $\tau$ ,

$$F^\Psi(t) \sim \begin{cases} \frac{4}{\tau} |\langle \psi_d | \psi_{in} \rangle|^2 e^{-4t/\tau} + 4\tau \left| \sum_{l=1}^{w-1} \lambda_l \theta_l e^{-t(\lambda_l \tau + i\omega_l)} \right|^2 \\ \frac{4}{\tau} e^{-4t/\tau} + \tau^3 \left| \sum_{l=1}^{w-1} \lambda_l e^{-t(\lambda_l \tau + i\omega_l)} \right|^2 \end{cases}, \quad (63)$$

where the first line holds for the transition problem and the second line for the return problem.

Integration of the PDF gives the following values for  $P_{\text{det}}^\Psi$  and the moments  $\langle T \rangle^\Psi$  in the Zeno limit:

$$P_{\text{det}}^\Psi \sim \begin{cases} |\langle \psi_d | \psi_{in} \rangle|^2 + \sum_{l=1}^{w-1} 2\lambda_l |\theta_l|^2, & |\psi_{in} \rangle \neq |\psi_d \rangle \\ 1, & |\psi_{in} \rangle = |\psi_d \rangle, \end{cases} \quad (64)$$

$$\langle T^m \rangle^\Psi \sim \begin{cases} \frac{m!}{P_{\text{det}}^\Psi} \sum_{l=1}^{w-1} \frac{2\lambda_l |\theta_l|^2}{(2\lambda_l \tau)^m}, & |\psi_{in} \rangle \neq |\psi_d \rangle \\ \delta_{m,1} \frac{\tau}{4} + \frac{m!}{4\tau^{m-2}} \sum_{l=1}^{w-1} \frac{2\lambda_l}{(2\lambda_l)^m}, & |\psi_{in} \rangle = |\psi_d \rangle. \end{cases} \quad (65)$$

The first measurement term is significant only for the first moment; otherwise it is negligible. Our Zeno limit reproduces the general results for the return problem, namely,  $P_{\text{det}}^\Psi(\psi_d) = 1$  and  $\langle T \rangle^\Psi = w\tau/4$ .

### B. Stroboscopic detection protocol

Given the connections found above between the NHH and stochastic protocol, we can read off the solution of the Zeno limit of the stochastic protocol. Of course, one can also approach the problem directly. To do this, it is necessary, as we did above in Sec. IV, to treat the first-detection attempt separately from the others. The other crucial step is to identify the poles  $z_l$  with the poles  $s_l$  of the non-Hermitian approach. The poles are determined by Eq. (38), but we will follow Sec. III and write  $z = e^{-s\tau}$ . Expanding for small  $\tau$  allows us to use Eq. (20) so that  $0 = 2u_\varphi(e^{-s\tau}) \sim 1 + 2u_\Psi(s)/\tau$ . This

means that we can use the poles  $s_l$  from Eq. (48), which we determined explicitly before, via

$$z_l \sim e^{-s_l \tau} \sim e^{\lambda_l \tau^2 + i\omega_l \tau} \quad (66)$$

for  $l = 1, \dots, w-1$ . As mentioned before, the poles  $s_l$  and  $z_l$  are related by our approximation procedure. A sketch can be found in Fig. 5.

The final pitfall we have to avoid is that  $0 = u_\varphi(z)$  has  $w-1$  solutions, but  $0 = 1 + 2u_\Psi(s)/\tau$  has  $w$  solutions. The non-Hermitian approach has one additional pole, namely, the fast mode  $s_0$ , that does not appear in the stroboscopic setup. The first measurement and  $\varphi_1$  play the role of the fast mode here. By simply excluding this spurious pole and using Eqs. (20), (21), (48), (55), (58), (59), and (66) in Eq. (41), one can arrive at the desired result:

$$\varphi_n \sim - \sum_{l=1}^{w-1} \frac{1}{\tau} \frac{v_\Psi(s_l) - \frac{\langle \psi_d | \psi_{in} \rangle}{2}}{\frac{d}{dz} u_\varphi(z)|_{z=e^{-s_l \tau}}} e^{(n+1)\tau s_l}$$

$$\sim \sum_{l=1}^{w-1} e^{-(n+1)\tau[\tau\lambda_l + i\omega_l]} \times \begin{cases} -2i\lambda_l \theta_l \tau, & |\psi_{in} \rangle \neq |\psi_d \rangle \\ -2\lambda_l \tau^2, & |\psi_{in} \rangle = |\psi_d \rangle. \end{cases} \quad (67)$$

These expressions for  $\varphi_n$  are plugged into the  $\delta$ -comb definition of  $F^\varphi(t) = \sum_{n=1}^{\infty} |\varphi_n|^2 \delta(t - n\tau)$ . The first-detection attempt remains untouched, but in the large- $n$  part, we replace the comb of  $\delta$  functions with a smooth function by writing  $\sum_{n=2}^{\infty} |\varphi_n|^2 \delta(t - n\tau) \sim |\varphi_{(t-\tau)/\tau}|^2 / \tau$ . This is equivalent to performing a local average of  $F^\varphi(t)$ . The additional shift is admissible when  $\tau$  is small. The result is

$$F^\varphi(t) \sim \begin{cases} |\langle \psi_d | \psi_{in} \rangle|^2 \delta(t - \tau) + 4\tau \left| \sum_{l=1}^{w-1} \lambda_l \theta_l e^{-t(\lambda_l \tau + i\omega_l)} \right|^2 \\ \delta(t - \tau) + 4\tau^3 \left| \sum_{l=1}^{w-1} \lambda_l e^{-t(\lambda_l \tau + i\omega_l)} \right|^2 \end{cases}, \quad (68)$$

where the first line is the result for the transition problem and the second line stands for the return problem. Integration of the density shows again the equivalence between both approaches. For the transition problem, we find the same result as in Eqs. (64) and (65). For the return problem, we find  $P_{\text{det}}^\varphi = P_{\text{det}}^\Psi = 1$  and the correction factor of 4,  $\langle T^m \rangle^\varphi = 4\langle T \rangle^\Psi$ , to Eq. (65).

We thus have found the Zeno limit of the first-detection time PDF for the stroboscopic detection protocol. Just like the Zeno limit of  $F^\Psi(t)$ , it consists of a ‘‘fast’’ part and a ‘‘slow’’ part. While the fast part in the stroboscopic detection protocol consists of the very first measurement, it takes the form of a quickly decaying exponential in the non-Hermitian setup. The fast dynamics cannot be compared, but the slow dynamics can easily be. In fact, they yield the exact same density, except for the return problem, where they differ by the factor of 4. Our Zeno limit reproduces nicely Eq. (30). We also recover the quantization of the mean in the return problem for both stroboscopic and non-Hermitian setups.

The just-derived PDF is plotted for the benzene ring and for the random Hamiltonian in Figs. 1(a) and 1(b). The figure

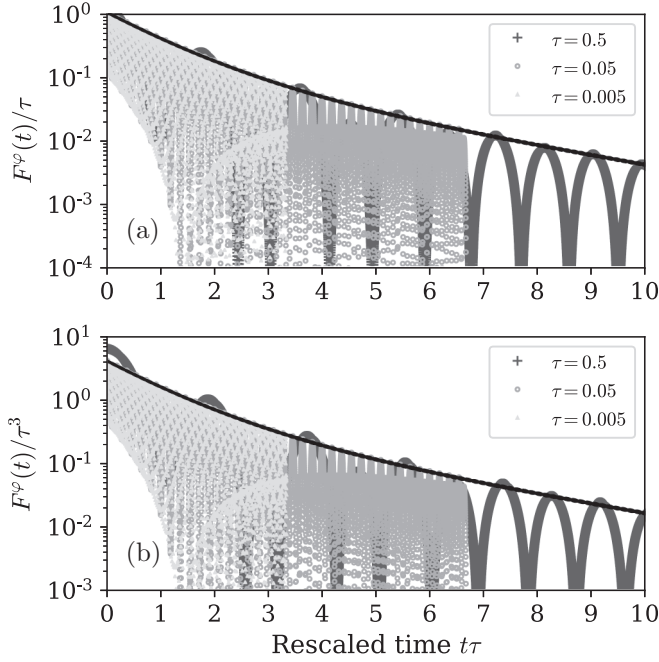


FIG. 7. Scaling form of the distribution  $F^\varphi(t)$  for the benzene ring  $\hat{H}_B$  [Eq. (31)]. Detection and initial states are like in Fig. 1. The distributions' envelopes for different  $\tau$  collapse onto each other. (Symbols are overlapping; time series are of different lengths.) The black solid line is a fit of the envelope. There is a different scaling of the prefactor in the return problem (b).

features a rather large value of  $\tau = 0.5$ , which has to be compared to the system's internal timescale  $\hbar/(E_{\max} - E_{\min}) = 0.25$ . Although  $\tau$  is rather large, the curves match quite well. The total detection probability and the moments for these models are plotted in Figs. 3 and 4. In all figures, the Zeno limit data are depicted by green circles and describes the stroboscopic data very well for small  $\tau$ .

Furthermore, we find that the slow part of  $F^\varphi(t)$  has a very particular scaling in  $t\tau$ . This is best seen in its envelope, when the oscillating terms  $e^{i(\omega_l - \omega_{l'})t}$  are neglected. This envelope is a scaling function  $C(\tau)f(t\tau)$ , where the prefactor is either  $\tau$  or  $\tau^3$ , depending on whether  $|\psi_{\text{in}}\rangle \neq |\psi_{\text{d}}\rangle$  or not. As a consequence, we can find a data collapse of the PDFs' envelopes of different values for  $\tau$ . This is demonstrated in Fig. 7. This particular scaling with  $t\tau$  was also reported in Refs. [18,25,36]. The  $t\tau$  scaling in the PDF impacts how the moments vary with  $\tau$ . Namely, we find that  $\langle T^m \rangle \propto \tau^{-m}$  for the transition problem and  $\langle T^m \rangle \propto \tau^{2-m}$  for the return problem. Higher moments diverge as  $\tau$  goes to zero, because the dissipation becomes much faster than the internal system dynamics. This is a manifestation of the Zeno effect. For very small  $\tau$ , the part of the wave function that was prepared in  $|\psi_{\text{d}}\rangle$ , namely,  $|\langle \psi_{\text{d}} | \psi_{\text{in}} \rangle|^2$ , is immediately detected; this is the meaning of the  $\delta$  functions in the distributions. The remaining amplitude in the system must be transferred to the detection state, but is reflected off it most of the time. Detection events that do not take place immediately after preparation are actually very rare and drive the blowup of the higher moments for small  $\tau$ .

## VIII. IN THE VICINITY OF THE RETURN PROBLEM

In the previous sections we highlighted the special place that the return problem takes among all other initial conditions. This manifests particularly in the quantized mean first-detection time. Its behavior switches from linear,  $\langle T \rangle^\varphi \propto \tau$ , to diverging,  $\langle T \rangle^\varphi \propto \tau^{-1}$ , depending on the initial state. Clearly, the return problem is on a somewhat delicate balance, which is easily perturbed by small alterations of the initial state or by imperfections in the detection protocol. In this section we explore the sensitivity or robustness of the return problem and in what sense the non-Hermitian and Zeno limit are applicable.

### A. Robustness of the return problem

How resilient are the return statistics to small changes in the initial state? When the initial state is equal to or very close to the detection state, most detection events will occur at  $n = 1$ , shortly after preparation. To explore this regime, we consider the mean first-detection time  $\langle T \rangle_\epsilon^\varphi$  for an initial state of the form

$$|\psi_{\text{in}}^\epsilon\rangle := \sqrt{1 - \epsilon^2}|\psi_{\text{d}}\rangle + \epsilon|\psi_{\text{in}}\rangle, \quad (69)$$

with, obviously,  $0 = \langle \psi_{\text{in}} | \psi_{\text{d}} \rangle$ . When  $\epsilon$  vanishes, this initial state describes the return problem. As  $\epsilon$  increases, we move towards the transition problem.

For small  $\tau$ , the mean first-detection time is a good observable to describe the contrast between transition and return problems, because of its high sensitivity. Figure 8(a) shows the  $\epsilon$  dependence of the mean for different values of  $\tau$  in the benzene ring. It also shows the non-Hermitian result  $\langle T \rangle^\Psi$ , which nicely describes the stroboscopic data for large  $\epsilon$ , but which settles at a fourth of the stroboscopic value when  $\epsilon$  goes to zero, nicely demonstrating the necessity of the correction factor in the return problem. Furthermore, we plotted the Zeno approximation of Eq. (65) that also matches the stroboscopic data for large  $\epsilon$ , but completely fails to describe  $\langle T \rangle_\epsilon^\varphi$  for small  $\epsilon$ , close to the return problem. The reason is that the transition times  $\theta_l = \theta_l(\psi_{\text{in}}^\epsilon)$  in Eq. (65) that determine the Zeno limit of  $\langle T \rangle_\epsilon^\varphi$  vanish as  $\epsilon$  goes to zero and  $\tau$  stays small but fixed. Figure 8(b) depicts the  $\epsilon$  dependence of the ratio  $\langle T \rangle_\epsilon^\varphi / \langle T \rangle_\epsilon^\Psi$  and shows explicitly how the correction factor of 4 emerges smoothly as soon as  $\epsilon$  becomes of the  $O(\tau)$  or smaller.

This is nicely demonstrated in a two-level system where  $\hat{H} = -2\gamma\hat{\sigma}_x$  is proportional to the Pauli- $x$  matrix. When  $|\psi_{\text{d}}\rangle$  and  $|\psi_{\text{in}}^{\epsilon=1}\rangle$  are given by the two states in the system, one finds

$$\frac{\langle T \rangle_\epsilon^\varphi}{\langle T \rangle_\epsilon^\Psi} \sim \frac{2 + \frac{\hbar^2}{4\gamma^2} \left(\frac{\epsilon}{\tau}\right)^2}{\frac{1-\epsilon^2}{2} + \frac{\hbar^2}{4\gamma^2} \left(\frac{\epsilon}{\tau}\right)^2}, \quad \tau \rightarrow 0. \quad (70)$$

Clearly, this ratio approaches 4 and 1 in the limits  $\epsilon \rightarrow 0$  and  $\epsilon/\tau \rightarrow \infty$ , respectively. The exact form of this ratio and in particular the width of the boundary layer around  $\epsilon \approx 0$  depend on the system details, but the scaling limits are universal.

When  $\epsilon$  and  $\tau$  are simultaneously small they compete with each other and the limits  $\epsilon \rightarrow 0$  and  $\tau \rightarrow 0$  do not commute. This is why the non-Hermitian and Zeno limits cannot agree for small  $\epsilon$ . Still, using asymptotic matching, one can compute a uniform Zeno limit that reproduces the stroboscopic data

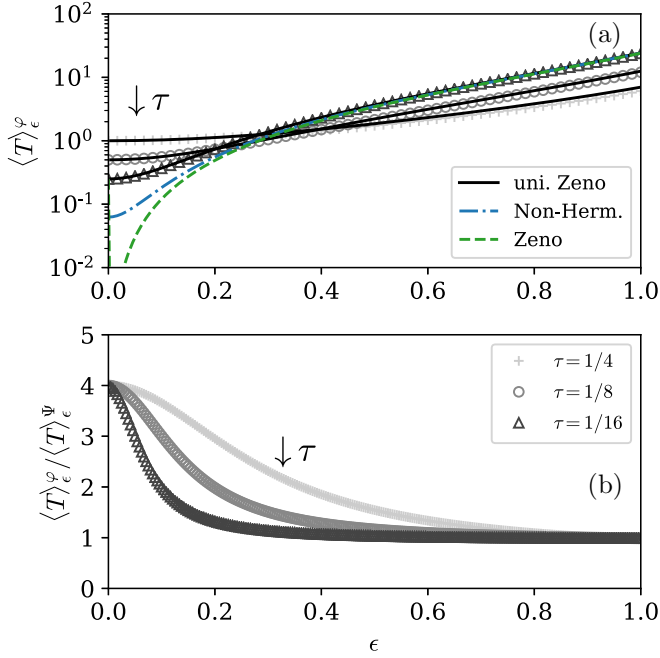


FIG. 8. Perturbation of the initial state in the benzene ring with  $|\psi_d\rangle = |0\rangle$  [see Eq. (69)]. (a) and (b): Gray symbols give the stroboscopic data for  $\tau = 1/4$  (+),  $1/8$  (o), and  $1/16$  ( $\Delta$ ), from top to bottom on the left-hand side. (a) Dashed and dash-dotted lines give the Zeno approximation (65) and the non-Hermitian data result (30), respectively, for  $\tau = 1/16$ . Both depart from the stroboscopic result close to the return problem (small  $\epsilon$ ). The uniform Zeno result [black solid line, Eq. (73)] matches the stroboscopic data perfectly for small  $\tau$ . (b) Ratio of the stroboscopic and non-Hermitian results. The correction factor of 4 emerges smoothly as  $\epsilon$  becomes smaller; however, significant deviations only start to occur for  $\epsilon = O(\tau)$ .

also for small  $\epsilon$  [see Fig. 8(a)]. Note that most of the previous sections' machinery still applies, because we only changed the initial state. When repeating the calculations from before with the initial state of Eq. (69), we need to take care with the quantity

$$v_\psi(\bar{s}_l) - \frac{\tau}{2} \langle \psi_d | \psi_{in}^\epsilon \rangle \sim \begin{cases} -i\epsilon\theta_l, & \tau \ll \epsilon \\ -\tau [1 + i\frac{\epsilon}{\tau}\theta_l], & \tau \approx \epsilon, \end{cases} \quad (71)$$

where now  $\theta_l = \theta_l(\psi_{in}^{\epsilon=1})$  coincides with the definition (59). Both equations are derived for small  $\tau$ , but the second alternative holds when  $\epsilon$  is also small and comparable to  $\tau$ . With this result we find

$$\langle T^m \rangle_\epsilon^\varphi \sim \begin{cases} \frac{\epsilon^2 \frac{m!}{\tau^m} \sum_{l=1}^{w-1} \frac{2\lambda_l |\theta_l|^2}{(2\lambda_l)^m}}{|\langle \psi_d | \psi_{in}^\epsilon \rangle|^2 + \epsilon^2 \sum_{l=1}^{w-1} 2\lambda_l |\theta_l|^2}, & \tau \ll \epsilon \\ \tau^m + \frac{m!}{\tau^{m-2}} \sum_{l=1}^{w-1} \frac{2\lambda_l |1 + i\frac{\epsilon}{\tau}\theta_l|^2}{(2\lambda_l)^m}, & \tau \approx \epsilon. \end{cases} \quad (72)$$

Thus, when  $\tau$  is much smaller than the distance  $\epsilon$  between the initial and detection states, the moments resemble those of the transition problem. When  $\tau$  and  $\epsilon$  are both small, we obtain an interpolation between the return and transition problems.

A uniform Zeno limit is achieved by the technique of asymptotic matching that combines both lines via  $\langle T \rangle_{\epsilon, \text{uni}} \sim \langle T \rangle_{\text{large } \epsilon} + \langle T \rangle_{\text{small } \epsilon} - \lim_{\epsilon \rightarrow 0} \langle T \rangle_{\text{large } \epsilon}$ , where

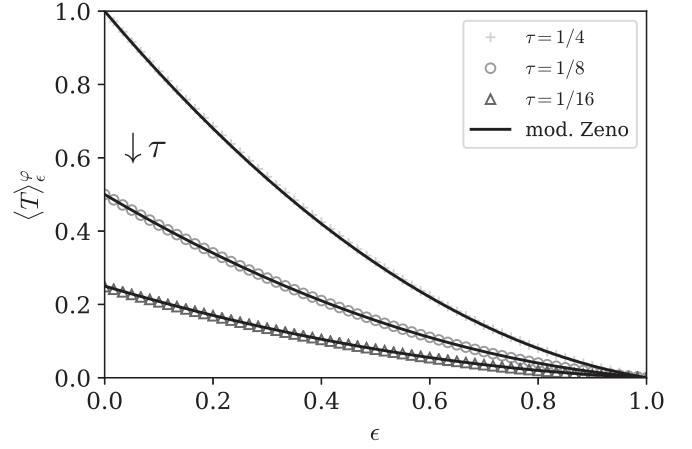


FIG. 9. Variation of the stroboscopic detection protocol by modifying the time of the first-detection attempt to be  $(1 - \epsilon)\tau$  in the benzene ring with  $|\psi_d\rangle = |0\rangle$ . Gray symbols give the stroboscopic data for  $\tau = 1/4$  (+),  $1/8$  (o), and  $1/16$  ( $\Delta$ ), from top to bottom on the left-hand side. The solid line gives the modified Zeno limit described in the text.

$\lim_{\epsilon \rightarrow 0} \langle T \rangle_{\text{large } \epsilon}$  is the small- $\epsilon$  expansion of the first line

$$\langle T^m \rangle_{\epsilon, \text{uni}}^\varphi \sim \tau^m + \frac{m!}{\tau^{m-2}} \sum_{l=1}^{w-1} \frac{2\lambda_l}{(2\lambda_l)^m} \left\{ \left| 1 + i\frac{\epsilon}{\tau}\theta_l \right|^2 + \frac{\epsilon^2 |\theta_l|^2}{|\langle \psi_d | \psi_{in}^\epsilon \rangle|^2 + \epsilon^2 \sum_{l=1}^{w-1} 2\lambda_l |\theta_l|^2} - \epsilon^2 |\theta_l|^2 \right\}. \quad (73)$$

This equation is used in Fig. 8(a) for  $m = 1$ , which matches the numerical data almost perfectly for small  $\tau$ . The main conclusion we can draw from this example is that the Zeno limit close to the return problem must be carefully performed, because the limits  $|\psi_{in}\rangle \rightarrow |\psi_d\rangle$  and  $\tau \rightarrow 0$  do not commute.

## B. Robustness of the detection protocol

In the same spirit as before, we can ask the question of how stable the return problem is to small disturbances in the detection protocol. We now consider a shift of the first-detection epoch by  $\epsilon\tau$ , with  $0 < \epsilon < 1$ , such that detection is attempted at  $(1 - \epsilon)\tau, (2 - \epsilon)\tau, \dots$ . This scheme is an interpolation between our stroboscopic detection protocol ( $\epsilon = 0$ ) and the scheme considered in Ref. [11], where the first-detection attempt occurs directly after preparation.

Again we investigate the mean  $\langle T \rangle_\epsilon^\varphi$  in the return problem. In the return problem, we find  $\langle T \rangle_{\epsilon=0}^\varphi = w\tau$ , but  $\langle T \rangle_{\epsilon=1}^\varphi = 0$ , because the system is detected directly after preparation. As  $\epsilon$  varies, one interpolates between both results continuously, as depicted in Fig. 9 for different values of  $\tau$ .

A formula for  $\langle T^m \rangle_\epsilon^\varphi$  in the Zeno limit is easily found. Reworking the argument in Sec. IV, we have that the probability of surviving the first measurement is now reduced by a factor of  $(1 - \epsilon)^2$ , since less probability has been transferred off the detection site before measurement. Similarly, the modified amplitude of the first successful detection at the  $n$ th attempt ( $n > 1$ ) is reduced by the same factor, as are all the moments of the first-detection time. The mean is plotted in Fig. 9,

where it agrees well with the numerical data. The result is an interpolation between the usual return result, namely, four times Eq. (65), and zero. For the first moment this gives  $\langle T \rangle_\xi^\varphi \sim (1 - \epsilon)[\epsilon + w(1 - \epsilon)]\tau$ , as  $\tau \rightarrow 0$ . For the perturbed detection protocol, there is no competition between  $\epsilon$  and  $\tau$ , as the latter only appears in the product  $(1 - \epsilon)\tau$ .

## IX. SUMMARY AND DISCUSSION

The quantum first-detection problem assesses the statistics of the first successful of many repeated detection attempts in the state  $|\psi_d\rangle$  performed stroboscopically with frequency  $1/\tau$ . The non-Hermitian Schrödinger equation (1) is an alternative model, where the projective measurements are replaced by an imaginary potential on  $|\psi_d\rangle$ . We presented the formal solutions to both problems and compared them with each other in the limit of small  $\tau$ . It was demonstrated that they then both yield the same statistics, except in the return problem,  $|\psi_{\text{in}}\rangle = |\psi_d\rangle$ , which necessitates an adjustment to restore the equivalence. This was also shown in extensive numerical simulations. For systems with a discrete energy spectrum, we presented another formal solution in terms of the poles  $\beta_l$  of the generating function  $\varphi(z)$  or the poles  $\mathfrak{s}_l$  of the Laplace transformed wave function  $\Psi(s)$ . The poles can be obtained from the stationary points of an electrostatic potential in both situations. It was demonstrated that the mean first-detection time  $\langle T \rangle$  is quantized for the return problem, rederiving the result of [15]. The relevant integer is  $w$ , the number of energy levels that appear in the spectral decomposition of  $|\psi_d\rangle$ . Using the electrostatic analogy, we found the Zeno limit  $\tau \rightarrow 0$  of the non-Hermitian description. Finally, using the Zeno limit, we analyzed the stroboscopic detection protocol in the vicinity of the return problem.

Throughout this article, we considered the simultaneous limit  $\tau \rightarrow 0$  and  $n \rightarrow \infty$ . Our technique here was anticipated in Ref. [25]. This way, we avoided the trivial result  $\varphi_n \sim \delta_{n,1} |\langle \psi_d | \psi_{\text{in}} \rangle|^2$  from Eq. (11), where all dynamical information is lost. Still, as is evident from the nature of the limit, we cannot map the region  $t \approx 0$ , where  $n = t/\tau$  is actually not large. The discrepancy between the fast parts in Eqs. (63) and (68) is a symptom of this inability. This discrepancy in the fast dynamics can also be expected from how the two models behave for small times as addressed in Sec. IV. Still, when comparing the actual probabilities of early detection from Eqs. (63) and (68), we find pretty good agreement: The relative error between  $\int_0^\tau dt F^\Psi(t)$  and  $\int_0^\tau dt F^\varphi(t)$  is approximately 2%.

Our approximation scheme  $z = e^{-s\tau}$  with a subsequent small- $\tau$  expansion is similar to the Tustin or bilinear transformation in signal theory [84]. This becomes clearer when  $z = e^{-s\tau} \sim (1 - \frac{s\tau}{2}) / (1 + \frac{s\tau}{2})$  is replaced by its Padé approximation. The Tustin transform is used to transform continuous-time filters into discrete-time ones and vice versa. It captures the low-frequency behavior correctly, but distorts the high frequencies, a phenomenon known as frequency warping, which makes resonant detection periods impossible in the non-Hermitian limit. The first resonant detection period, defined by  $\tau_c = 2\pi\hbar / (E_{\text{max}} - E_{\text{min}})$ , therefore poses a hard limit for the validity of the non-Hermitian description. This is well supported by our numerical data.

The relevance of certain poles in our formalism, as well as the interpretation of their (or their logarithm's) real and imaginary parts as lifetimes and frequencies, is reminiscent of the quantum resonance framework [85,86]. In fact, similar to the theory of Feshbach resonances [87], we solved the Laplace-transformed (i.e., stationary) Schrödinger equation by substituting the  $[\mathbb{1} - \hat{D}]$  projection into the  $\hat{D}$  component in Sec. II. In Secs. VI and VII we used the fact that discrete states give rise to poles in the solution which control the dynamics. A similar procedure was applied to the renewal equation (12) that yields the generating function  $\varphi(z)$ . However, despite these formal similarities, our aim was somewhat different from classical scattering theory: We were interested in the distribution and statistics of the first-detection time.

When we derived  $P_{\text{det}}^\varphi$  in the Zeno limit in Eq. (64), we encountered  $|\langle \psi_d | \psi_{\text{in}} \rangle|^2$ . This is the probability of detection directly after preparation. Further,  $P_{\text{det}}^\varphi(\psi_{\text{in}}) - |\langle \psi_d | \psi_{\text{in}} \rangle|^2 = \sum_{l=1}^{w-1} 2\lambda_l |\theta_l|^2$  is the difference in the total detection probability between the stroboscopic detection protocol and a “one-shot” detection protocol. In Refs. [27,28] we demonstrated that this quantity can be bounded by an uncertainty relation so that

$$P_{\text{det}}^\varphi(\psi_{\text{in}}) - |\langle \psi_d | \psi_{\text{in}} \rangle|^2 = \sum_{l=1}^{w-1} 2\lambda_l |\theta_l|^2 \geq \frac{|\langle \psi_d | [\hat{H}\hat{D}] | \psi_{\text{in}} \rangle|^2}{\text{Var}[\hat{H}]_{\psi_d}}, \quad (74)$$

where  $\hat{D} := |\psi_d\rangle\langle\psi_d|$  and  $\text{Var}[\hat{H}]_{\psi_d} := \langle \psi_d | \hat{H}^2 | \psi_d \rangle - [\langle \psi_d | \hat{H} | \psi_d \rangle]^2$  are the energy fluctuations in the detection state.

The special character of the return problem, in particular the quantization of the mean first return time, was already discussed and recognized for the stroboscopic detection protocol [15,22,23]. The quantization for the non-Hermitian Schrödinger equation will be showcased in a separate work [29].

In many realistic situations there is more than one target state  $|\psi_d\rangle$ , but rather a target (sub)space  $\hat{D}\mathcal{H}$  of the total Hilbert space  $\mathcal{H}$ , where  $\text{rank } \hat{D} \geq 1$ . For the sake of simplicity, this situation was avoided in this paper, because the formal solutions become somewhat more involved. In particular, one has to replace the weights or charges with  $p_l q_l \mapsto \hat{D}\hat{P}_l|\psi_{\text{in}}\rangle$  and  $p_l \mapsto \hat{D}\hat{P}_l\hat{D}$  such that the functions  $v_\psi(s)$  and  $v_\varphi(z)$  become vector valued and  $u_\psi(s)$  and  $u_\varphi(z)$  become matrix valued. Apart from the mathematical issue, there is the following qualitative physical question (see also Ref. [88]): *Where* in the detection subspace does the system arrive? We believe that this will lead to richer dynamics, but not too many conceptual differences, provided  $\text{rank } \hat{D} < \infty$ . Reference [16] investigated the return problem in the stroboscopic approach and showed that the mean return time is quantized provided that the system is prepared in the mixed state  $\hat{\rho}_{\text{in}} = \hat{D}/\text{rank}[\hat{D}]$ . Therefore, in this sense the return problem retains its special status and we can expect a correction factor to appear also in the higher-dimensional case.

Experimental verification of our claims is well within reach. In fact, Ref. [89] reports an experiment of a photonic quantum walk on the line in which  $P_{\text{det}}$  has been measured with the stroboscopic approach. Apart from discrete-time quantum walks, cold-atom experiments provide the optimal

test bed for our theory. Reference [78] implements a continuous-time quantum walk of cold atoms in momentum space, whereas Ref. [79] uses hyperfine levels of lithium. In both cases, detection or loss is implemented by resonant coupling of the principal system to some “sink” at some (target) state, from which return is unlikely. Population measurements of the reservoir or, alternatively, the sink at time  $t$  give the probability of survival  $S(t) = \int_t^\infty dt' F(t')$ . A pulsed system-sink coupling then realizes the stroboscopic approach, whereas continuous coupling realizes the non-Hermitian scenario.

We have demonstrated that the analogy between the non-Hermitian Schrödinger equation and the stroboscopic detection protocol is very delicate. The equivalence of both depends crucially on the value of  $\tau$ , the exact definition of the detection protocol, and the initial state in question. In the vicinity of the return problem, both the Zeno and non-Hermitian approximations are particularly untrustworthy. This shows that the first-detection statistics may be quite sensitive to their exact operational definition. The popular non-Hermitian description must be motivated with great care to detail in any repeated measurement setup.

#### ACKNOWLEDGMENTS

F.T. is grateful to Deutsche Forschungsgemeinschaft (DFG, Germany) for support under Grants No. TH 2192/1-1 and No. TH 2192/2-1. Support from Israel Science Foundation through Grant No. 1898/17 is acknowledged.

#### APPENDIX A: ADIABATIC ELIMINATION OF THE FAST MODE

Following Dhar *et al.* [19], we show in this Appendix how to obtain another non-Hermitian equation with a small optical potential from Eq. (1). This is achieved via adiabatic elimination of the fast mode. Starting from Eq. (1), we decompose the wave function into two orthogonal parts  $|\psi(t)\rangle = |\psi_d\rangle\Psi(t) + |\bar{\psi}(t)\rangle$  such that  $\hat{D}|\bar{\psi}(t)\rangle = 0$ . We assume that the initial state has no overlap with  $|\psi_d\rangle$ ,  $\langle\psi_d|\psi_{\text{in}}\rangle = 0$ . After Laplace transformation, the Schrödinger equation reads, in block form,

$$is\Psi(s) = \left[ \langle\hat{H}\rangle - \frac{2i}{\tau} \right] \Psi(s) + \langle\psi_d|\hat{H}(\mathbb{1} - \hat{D})|\bar{\psi}(s)\rangle, \quad (\text{A1a})$$

$$i[s|\bar{\psi}(s)\rangle - |\psi_{\text{in}}\rangle] = (\mathbb{1} - \hat{D})\hat{H}|\psi_d\rangle\Psi(s) + \hat{H}_Z|\bar{\psi}(s)\rangle, \quad (\text{A1b})$$

where  $\langle\hat{H}\rangle = \langle\psi_d|\hat{H}|\psi_d\rangle$  and  $\hat{H}_Z := (\mathbb{1} - \hat{D})\hat{H}(\mathbb{1} - \hat{D})$  is the Zeno Hamiltonian (see [81]). Solving Eq. (A1a) for  $\Psi(s)$  and plugging the result into Eq. (A1b) yields

$$i[s|\bar{\psi}(s)\rangle - |\psi_{\text{in}}\rangle] = \left[ \hat{H}_Z + \frac{\hat{H}_1}{is - \langle\hat{H}\rangle + \frac{2i}{\tau}} \right] |\bar{\psi}(s)\rangle, \quad (\text{A2})$$

where  $\hat{H}_1 = (\mathbb{1} - \hat{D})\hat{H}\hat{D}(\mathbb{1} - \hat{D})$ . When  $\tau$  is very small, the terms  $is - \langle\hat{H}\rangle$  can be neglected in the denominator and we obtain an effective non-Hermitian Hamiltonian that only acts on the subspace  $(\mathbb{1} - \hat{D})$ . An inverse Laplace transform gives

the effective Schrödinger equation

$$i\hbar \frac{d}{dt} |\bar{\psi}(t)\rangle = \left[ \hat{H}_Z - i \frac{\tau}{2\hbar} \hat{H}_1 \right] |\bar{\psi}(t)\rangle. \quad (\text{A3})$$

This is exactly the equation used in Refs. [18–20,54].

#### APPENDIX B: LAZY DETECTOR LIMIT

In Sec. VII we derived the Zeno limit for the non-Hermitian Schrödinger equation. This was achieved by a perturbation of the equation  $0 = 1 + 2u_\Psi(s)/\tau$  as  $\tau \rightarrow 0$ . A similar procedure is possible in the opposite limit  $\tau \rightarrow \infty$ , when the detector becomes slower and slower. Obviously, this has no correspondence to the stroboscopic detection protocol, whence we omitted its discussion in the main text. Nevertheless, it is clearly justified as a proper non-Hermitian system with a very weak dissipation term, which is why we present it here. The general considerations of Sec. VI still hold. Thus, it is only necessary to find the poles  $\bar{s}_l$  in this limit.

When  $\tau$  becomes large in  $0 = 1 + 2u_\Psi(s)/\tau$ ,  $u_\Psi(s)$  must become large as well to satisfy the equation. For this reason, we expand  $u_\Psi(s)$  around its singularities  $s = -iE_l/\hbar$ , by making the ansatz  $\bar{s}_l \sim -i(E_l/\hbar) - (a_l/\tau)$  for  $l = 1, \dots, w$ . Plugging this ansatz into Eq. (48) together with Eq. (47) reveals  $a_l = p_l$ . That means we find

$$\bar{s}_l \sim -\frac{2p_l}{\tau} - i\frac{E_l}{\hbar}, \quad l = 1, \dots, w. \quad (\text{B1})$$

The same result is obtained when one applies regular perturbation theory to find the eigenvalues  $\tilde{E}_l(\tau) = -i\hbar\bar{s}_l$  of Eq. (1).

Plugging these poles into the functions  $v_\Psi(s)$  and  $u_\Psi(s)$ , we obtain in leading order

$$v_\Psi(\bar{s}_l) \sim q_l, \quad u'_\Psi(\bar{s}_l) \sim -\frac{\tau^2}{4p_l}. \quad (\text{B2})$$

With these we obtain  $\Psi(s)$  from Eq. (50),

$$\Psi(t) \sim \sum_{l=1}^w p_l q_l e^{-t[2p_l/\tau + iE_l/\hbar]}. \quad (\text{B3})$$

Integration of  $F^\Psi(t) = 4|\Psi(t)|^2/\tau$  yields the total detection probability and the moments. In leading order in  $\tau \rightarrow \infty$ , these are independent of the energy levels  $E_l$  and just depend on the charges  $p_l$  and  $q_l$ ,

$$P_{\text{det}} \sim \sum_{l=1}^w p_l |q_l|^2, \quad (\text{B4})$$

$$\langle T^m \rangle \sim m! \frac{\tau^m}{4^m} \frac{\sum_{l=1}^w p_l |q_l|^2 p_l^{-m}}{\sum_{l=1}^w p_l |q_l|^2}. \quad (\text{B5})$$

It is not obvious that the here-derived normalization for  $\tau \rightarrow \infty$  coincides with the  $\tau \rightarrow 0$  limit of Eq. (64). However, judging from our numerical simulations depicted in Figs. 3 and 4, which show perfect constancy in  $P_{\text{det}}^\Psi(\tau)$ , we can conclude that they are the same. Furthermore, it correctly reproduces the exact result for the stroboscopic detection protocol of Ref. [28]. We also reproduce the quantization of the return problem for large  $\tau$ :  $\langle T \rangle = w\tau/4$ .

Another remark on Eq. (B3) is called for. In contrast to the small- $\tau$  expansion of the main text, we find the unified

scaling  $F^\Psi(t) = \tau^{-1} f(t/\tau)$  for the envelope here. There is no separation between a fast and some slow modes. All modes' timescales are of the same order of magnitude  $\tau$ .

### APPENDIX C: CALCULATIONS FOR THE INFINITE LINE

In this Appendix we explain how all quantities pertaining to the infinite line Hamiltonian (32) have been obtained. To simplify our equations, we work in units of time where  $\hbar/\gamma = 1$ . Furthermore, we will use the abbreviation  $\Gamma = 2/\tau$  when convenient. We will make heavy use of the techniques of Krapivsky *et al.* described in Ref. [59], repeating some of their calculation, but also expanding upon them.

Reference [24] reported the transition amplitudes for this model:

$$\langle x|\hat{U}(t)|y\rangle = i^{|x-y|} J_{|x-y|}(2t). \quad (\text{C1})$$

Here  $J_n(x)$  is the Bessel function of the first kind and  $\hat{U}(t) = e^{-it\hat{H}/\hbar}$ . Henceforth, we write  $\xi = |x - y|$ . This expression is plugged into  $[s + i\hat{H}/\hbar]^{-1} = \int_0^\infty dt e^{-st - it\hat{H}/\hbar}$  to obtain the resolvent of the Hamiltonian

$$\langle x|\frac{1}{s + \frac{i}{\hbar}\hat{H}}|y\rangle = \frac{[\frac{i}{2}(\sqrt{4+s^2} - s)]^\xi}{\sqrt{4+s^2}}, \quad (\text{C2})$$

where Eq. (6.611.1) of [90] was used. We consider the detection state  $|\psi_d\rangle = |0\rangle$  and the initial state  $|\psi_{in}\rangle = |\xi\rangle$ . Therefore, above expression gives  $v_\Psi(s)$  and also  $u_\Psi(s)$  upon setting  $\xi = 0$ . This results in

$$\Psi_\xi(s) = \frac{[\frac{i}{2}(\sqrt{4+s^2} - s)]^\xi}{\Gamma + \sqrt{4+s^2}}. \quad (\text{C3})$$

The initial state is carried in a subscript from here on.

We will first find an expression for  $\Psi(t)$  in time domain and then proceed to compute the first moment of  $\langle T \rangle^\Psi$ .

#### 1. Wave function in time domain

In the return problem  $\xi = 0$ ,  $\Psi_0(s)$  is a function of  $\sqrt{1 + s^2/4}$  only. By virtue of Eq. (1.1.1.37) of [91], we thus find

$$\Psi_0(t) = e^{-\Gamma t} - 2t \int_0^1 dy J_1(2ty) e^{-\Gamma \sqrt{1-y^2}}. \quad (\text{C4})$$

The remaining integral can be obtained numerically.

For the transition case  $\xi \neq 0$ , we use Eq. (2.9.1.15) of [91] to identify the numerator of Eq. (C3) with  $i^\xi \xi J_\xi(2t)/2t$ . The denominator is the same expression as before; their product becomes a convolution in the time domain

$$\Psi_\xi(t) = \frac{\xi}{2} i^\xi \int_0^t dt' \frac{J_\xi(2(t-t'))}{t-t'} \Psi_0(t'). \quad (\text{C5})$$

$$P_{\text{det}}(\tau) = \begin{cases} \frac{2}{\pi} \frac{1}{\tau^2(1-\tau^2)} \{(\pi - 2\tau)(1 - \tau^2) + \tau^3 - [2(1 - \tau^2)^2 + \tau^2] \frac{\arccos \tau}{\sqrt{1-\tau^2}}\}, & |\psi_{in}\rangle = |1\rangle \\ \frac{1}{\pi} \frac{2\tau}{1-\tau^2} [1 + \frac{1-2\tau^2}{\tau} \frac{\arccos \tau}{\sqrt{1-\tau^2}}], & |\psi_{in}\rangle = |0\rangle. \end{cases} \quad (\text{C12})$$

These are the curves plotted in Fig. 2 for the non-Hermitian Schrödinger equation. The corrected non-Hermitian data were obtained from Eq. (C12) as well via  $4P_{\text{det}}^\Psi - 3$  [see Eq. (30)].

The  $\Psi_\xi(t)$  can be obtained by numerical quadrature of the last two integrals. Note that we can take the limit  $\tau \rightarrow 0$  in Eq. (C4) to obtain the much simpler result

$$\Psi_\xi(s) \sim i^\xi \frac{\tau}{2} \left[ \sqrt{1 + \frac{s^2}{4}} - \frac{s}{2} \right]^\xi, \quad (\text{C6})$$

which transforms to

$$\Psi_\xi(t) \sim i^\xi \frac{\xi \tau}{2t} J_\xi(2t) \quad (\text{C7})$$

and recovers our result from Ref. [25].

#### 2. Total detection probability

From Eq. (5), the total detection probability and the moments are given by a contour integral. However, careful attention must be paid to the branch cuts of the square-root function. Equation (5) is derived from the following identity:  $P_{\text{det}}^\Psi = \lim_{\epsilon \searrow 0} \int_0^\infty dt e^{-\epsilon t} 2\Gamma [\Psi(t)]^* \Psi(t)$ . Writing  $\Psi(t) = \int_{\mathcal{B}} ds e^{st} \Psi(s)/2\pi i$  and switching the order of integration, one finds

$$P_{\text{det}}^\Psi \langle T^m \rangle^\Psi = \lim_{\epsilon \searrow 0} 2\Gamma \int_{\mathcal{B}} \frac{ds}{2\pi i} \Psi^*(\epsilon - s) \Psi(s), \quad (\text{C8})$$

where  $0 < \text{Re}[s] < \epsilon$  so that all intermediary integrals converge. We thus parametrize the Bromwich path as  $s = \lambda + i\omega$ , with  $0 < \lambda < \epsilon$ , use the definition  $\Psi^*(s) = [\Psi(s^*)]^*$ , and take the limit  $\epsilon \rightarrow 0$ . This shows that both factors in the integrand must be evaluated at  $0^+ + i\omega$  and fixes the correct branch of the square-root function

$$P_{\text{det}}^\Psi = \frac{2\Gamma}{2\pi} \int_{-\infty}^{\infty} d\omega |\Psi(0^+ + i\omega)|^2. \quad (\text{C9})$$

The square-root functions in  $\Psi(s) = \Psi_\xi(s)$  are replaced by

$$\sqrt{4 + (0^+ + i\omega)^2} = i \text{sgn}(\omega) \sqrt{\omega^2 - 4} \quad (\text{C10})$$

for  $|\omega| > 2$  and the obvious limit  $\sqrt{4 - \omega^2}$  for  $|\omega| < 2$ . We abbreviate  $\delta := \text{sgn}(\omega) \sqrt{\omega^2 - 4}$  and  $\bar{\delta} := \sqrt{4 - \omega^2}$ . With this formula, we find that

$$|\Psi_\xi(0^+ + i\omega)|^2 = \begin{cases} \frac{1}{(\Gamma + \bar{\delta})^2}, & |\omega| \leq 2 \\ \frac{[\frac{1}{2}(\omega - \delta)]^{2\xi}}{\Gamma^2 + \delta^2}, & |\omega| > 2. \end{cases} \quad (\text{C11})$$

This expression is integrated over  $\omega$  from  $-\infty$  to  $\infty$  and multiplied by  $2\Gamma/2\pi$  to yield  $P_{\text{det}}^\Psi$ . This has already been done in Ref. [59], whose solution we here cite:

#### 3. Mean detection time

The mean detection time is computed in a similar manner to before. First, we note that the derivative of  $\Psi_\xi(s)$  can be

written as

$$-\frac{d\Psi_\xi(s)}{ds} = \Psi_\xi(s) \frac{s + \xi(\Gamma + \sqrt{4 + s^2})}{[4 + s^2] + \Gamma\sqrt{4 + s^2}}. \quad (\text{C13})$$

The procedure from before applied to Eq. (6) then yields

$$\langle T \rangle^\Psi = -\frac{1}{P_{\text{det}}^\Psi} \frac{2\Gamma}{2\pi i} \int_{-\infty}^{\infty} d\omega |\Psi_\xi(s)|^2 \frac{d \ln \Psi_\xi(s)}{ds} \Big|_{s=0^+ + i\omega}. \quad (\text{C14})$$

Combining Eqs. (C10), (C11), (C13), and (C14) and using the symmetry of the integrands gives  $\langle T \rangle^\Psi$  as a sum over two integrals, one over  $|\omega| < 2$  and one over  $|\omega| > 2$ :

$$\langle T \rangle^\Psi = \frac{2\Gamma}{2\pi P_{\text{det}}^\Psi} \left\{ \int_0^2 d\omega \frac{2\xi}{\delta(\Gamma + \delta)^2} + \int_2^\infty d\omega \frac{2\Gamma\omega \left[\frac{1}{2}(\omega - \delta)\right]^{2\xi}}{\delta(\Gamma^2 + \delta^2)^2} \right\}. \quad (\text{C15})$$

We call the integral in the first line  $I_1$  and the one in the second line  $I_2$ .

The first integral is solved by changing variables to  $\delta$  with  $d\delta = \omega d\omega/\delta$  and using *Mathematica*:

$$I_1 = \frac{1}{2\Gamma} \frac{2\xi\tau}{1 - \tau^2} \left[ \frac{\arccos(\tau)}{\sqrt{1 - \tau^2}} - \tau \right]. \quad (\text{C16})$$

$$\langle T \rangle^\Psi = \begin{cases} \frac{1}{P_{\text{det}}^\Psi(\xi=1)} \left\{ \frac{2-3\tau^2+\tau^2}{8\tau(1-\tau^2)^2} - \frac{1+\tau^2}{2\pi(1-\tau^2)} + \frac{1-3\tau^2}{2\pi\tau} \frac{\arccos(\tau)}{\sqrt{1-\tau^2}} \right\}, & |\psi_{\text{in}}\rangle = |1\rangle \\ \frac{1}{P_{\text{det}}^\Psi(\xi=0)} \frac{\tau}{8}, & |\psi_{\text{in}}\rangle = |0\rangle. \end{cases} \quad (\text{C19})$$

Combined with Eq. (C12), this result is plotted in Fig. 2.

#### 4. Total detection probability

The total detection probability for the NHH is given by Eq. (C12). Expanding the result for  $\xi = 0$  for small  $\tau$ , one obtains

$$P_{\text{det}}^\Psi = 1 - \frac{1}{4}\tau^2 + \frac{8}{3\pi}\tau^3 - \frac{9}{8}\tau^4 + \frac{64}{15\pi}\tau^5 - \frac{25}{16}\tau^6 + \dots \quad (\text{C20})$$

The first-detection amplitudes from the stroboscopic approach are obtained from the renewal equation and Eq. (C1). The first terms read

$$\varphi_n = \begin{cases} J_0(2\tau), & n = 1 \\ -\frac{2\tau}{n} J_1(2n\tau) - \frac{3\tau^2}{n^2} J_2(2n\tau) + \dots, & n > 1. \end{cases} \quad (\text{C21})$$

From this and  $P_{\text{det}}^\Psi = \sum_{n=1}^{\infty} |\varphi_n|^2$  we can compute the total detection probability in orders of  $\tau$ :

$$P_{\text{det}}^\Psi = 1 - 2\tau^2 + \frac{32\tau^3}{3\pi} - \frac{9\tau^4}{2} + \frac{256\tau^5}{15\pi} - \frac{50\tau^6}{9} + \dots \quad (\text{C22})$$

Comparing the expressions for the stroboscopic and the NHH approach, we see that, surprisingly, the ‘‘corrected’’ NHH result  $4P_{\text{det}}^\Psi - 3$  agrees with the stochastic result for the first five orders in  $\tau$ , disagreeing only at order  $\tau^6$ .

For the second integral, we use the variable transform  $\omega = 2 \cosh x$  such that  $\delta = 2 \sinh x$ ,  $\omega - \delta = 2e^{-x}$ , and  $d\omega = 2 \sinh x dx$ . This gives

$$I_2 = \int_2^\infty d\omega \frac{2\Gamma\omega \left[\frac{1}{2}(\omega - \delta)\right]^{2\xi}}{\delta(\Gamma^2 + \delta^2)^2} = \frac{\tau^2}{2\Gamma} \int_0^\infty dx \frac{e^{-2\xi x} \cosh x}{(1 + \tau^2 \sinh^2 x)^2}, \quad (\text{C17})$$

where we already replaced  $2/\Gamma = \tau$  for convenience. The exact integral is calculated with *Mathematica* and results in a complicated mix of polynomial and logarithmic terms in  $\tau$  for general  $\xi$ . For  $\xi = 0$  and  $\xi = 1$  the result is

$$I_2 = \begin{cases} \frac{1}{2\Gamma} \frac{\pi}{4} \tau, & \xi = 0 \\ \frac{1}{2\Gamma} \frac{\pi}{4} \frac{2+\tau^2}{\tau} - 1 - \frac{\arccos(\tau)}{\tau\sqrt{1-\tau^2}}, & \xi = 1. \end{cases} \quad (\text{C18})$$

Adding  $I_1$  and multiplying by  $2\Gamma/2\pi P_{\text{det}}^\Psi$  gives the conditional mean detection time

## APPENDIX D: DETAILS OF THE SIMULATIONS

In this Appendix we describe how the data for the figures were obtained.

### 1. Infinite line

#### a. Total detection probability and mean first-detection time

The total detection probability that is plotted in Fig. 2 was generated in the following way. The  $P_{\text{det}}^\Psi(\tau)$  was already computed in Ref. [59] for the infinite line. We repeated the result in Eq. (C12) and plotted these curves in Fig. 2. The corrected non-Hermitian data were obtained from Eq. (C12) as well via  $4P_{\text{det}}^\Psi - 3$  [see Eq. (30)]. The same was done for the mean, which we calculated in Eq. (C19).

The total detection probability and the mean first-detection time for the stroboscopic detection protocol were obtained from the renewal equation (12) and the exact expression (C1). The  $P_{\text{det}}^\Psi(\tau)$  was approximated by the sum  $\sum_{n=1}^N |\varphi_n|^2$ , where  $N$  was chosen such that the last summand was sufficiently small. The same approach was taken to compute  $\langle T \rangle \approx \sum_{n=1}^N |\varphi_n|^2 (n\tau) / P_{\text{det}}^\Psi(\tau)$ . This way the curves for the stroboscopic data in Fig. 2 were generated.

#### b. Probability density function

The stroboscopic data in Fig. 1(c) were generated from the renewal equation as explained above. Equation (C1) was used together with Eq. (12) to obtain  $\varphi_n$ . Still  $F^\Psi(t)$  contains the  $\delta$  functions  $\delta(t - n\tau)$ . To avoid them, we plotted the

local average  $(1/\tau) \int_{(n-1/2)\tau}^{(n+1/2)\tau} dt F^\varphi(t) = |\varphi_n|^2/\tau$  instead of  $F^\varphi(n\tau)$ . Hence, we used the data points  $(n\tau, |\varphi_n|^2/\tau)$  for the stroboscopic data, where  $\varphi_n$  was obtained as described above. The non-Hermitian data were obtained from numerical quadrature of Eqs. (C4) and (C5) that we derived above and from  $F(t) = (4/\tau)|\Psi(t)|^2$ .

## 2. Benzene ring

The ring Hamiltonian  $\hat{H}_B$  has four distinct energy levels that have overlap with  $|\psi_d\rangle$  and therefore  $w = 4$ . Both Hamiltonians have four energy levels which have overlap with  $|\psi_d\rangle$  and therefore  $w = 4$ . The resolvents  $u_\Psi(s)$  and  $u_\varphi(s)$  are found symbolically from the matrix representations (31) and from Eq. (33) using *Mathematica*. Since  $w$  is small enough, the poles  $\beta_l$  and  $\varepsilon_l$  can also be determined symbolically, as none of the polynomials encountered have order larger than 4.

### a. Probability density function

Using the exact expressions of the poles, of the resolvents, and of  $v_\Psi(s)$  as well as  $v_\varphi(z)$ , we can find  $\varphi_n$  and  $\Psi(t)$  from Eqs. (41) and (50). The expression we obtain for  $\varphi_n$  is a sum of exponential functions in  $n$ ,  $\varphi_n = f(n)$ . To compare it with the non-Hermitian data, we plotted  $F^\Psi(t) = 4|\Psi(t)|^2/\tau$  and  $F^\varphi(t) \approx |\varphi_{t/\tau}|^2/\tau = |f(t/\tau)|^2/\tau$  in Fig. 1. This is the interpolation that was mentioned in the caption of Fig. 1.

### b. Moments and total detection probability

The previous method was used to compute the moments for the non-Hermitian approach as well. The poles  $\varepsilon_l$ , as well as  $u'_\Psi(\varepsilon_l)$  and  $v_\Psi(\varepsilon_l)$ , were computed symbolically. From Eq. (50) we found

$$P_{\text{det}}^\Psi = \tau \sum_{l,l'=0}^{w-1} \frac{v_\Psi(\varepsilon_l)[v_\Psi(\varepsilon_{l'})]^* - 1}{u'_\Psi(\varepsilon_l)[u'_\Psi(\varepsilon_{l'})]^* \varepsilon_l + \varepsilon_{l'}^*}, \quad (\text{D1})$$

$$\langle T \rangle^\Psi = \frac{\tau}{P_{\text{det}}^\Psi} \sum_{l,l'=0}^{w-1} \frac{v_\Psi(\varepsilon_l)[v_\Psi(\varepsilon_{l'})]^* (-1)^m m!}{u'_\Psi(\varepsilon_l)[u'_\Psi(\varepsilon_{l'})]^* (\varepsilon_l + \varepsilon_{l'}^*)^{m+1}}. \quad (\text{D2})$$

The stroboscopic data were obtained from the quantum renewal equation (12) just like for the infinite line. The transition amplitudes were obtained numerically from the matrix form of the Hamiltonian. Having numerical values for  $\varphi_n$ ,

the non-normalized moments were obtained via  $\langle T^m \rangle^\varphi P_{\text{det}}^\varphi \approx \tau^m \sum_{n=1}^N n^m |\varphi_n|^2$ . Here  $N$  was chosen such that the last summand is small compared to the sum.

## 3. Random Hamiltonian

A slightly different approach was chosen for the random Hamiltonian  $\hat{H}_R$ . Here a complete symbolic computation of the resolvents was not possible, due to the large dimension of  $\hat{H}_R$ . Instead,  $\hat{H}_R$  was numerically diagonalized. Then it was renormalized via

$$\hat{H}_R \rightarrow \frac{4\gamma}{E_{\text{max}} - E_{\text{min}}} \left[ \hat{H}_R - \frac{E_{\text{max}} + E_{\text{min}}}{2} \mathbb{1}_{32} \right], \quad (\text{D3})$$

so that its eigenvalues lay in  $[-2\gamma, 2\gamma]$ .

The eigensystem contained all energy levels  $E_l$  and was also used to find the overlaps  $p_l$  and  $q_l$ . Having the overlaps and the energy levels, we computed the resolvents  $u_\Psi(s)$  [ $v_\Psi(s)$ ] semisymbolically in *Mathematica*. This allowed us to find the poles  $\varepsilon_l$  and from them  $\Psi(t)$  as well as all moments.

The stroboscopic PDF and the stroboscopic moments were obtained from the renewal equation. To achieve this, the transition and return amplitudes were computed from

$$\langle \psi_d | \hat{U}(n\tau) | \psi_{\text{in}} \rangle = \sum_l p_l q_l e^{-in(\tau E_l/\hbar)}, \quad (\text{D4})$$

and similarly for  $\langle \psi_d | \hat{U}(n\tau) | \psi_d \rangle$ . All required quantities were given by the eigensystem of  $\hat{H}_R$ . The non-normalized moments were obtained as described in the preceding section with  $N = 10000$ .

However, especially for small  $\tau$ , convergence was an issue. The convergence rate of the sum  $\sum_{n=1}^N f(n)|\varphi_n|^2$  is given by the largest modulus of the poles  $\max |\beta_l|$ . This in turn is controlled by the magnitude of the overlaps  $p_l$  and the distance between adjacent energy levels  $\Delta E_l = |E_{l+1} - E_l|$ . Since we did not want to choose a much larger  $N$ , we picked a realization of  $\hat{H}_R$  for Fig. 3 such that  $N^* := \max(\min p_l, \min \Delta E_l^2)$  was smaller than 1000. We estimated that roughly 20% of all matrices from the Gaussian unitary ensembles fall in this class. The results are qualitatively the same for every matrix of the ensemble. For matrices with a large  $N^*$  (and summation with a fixed  $N$ ) there will be a more severe dip in the stroboscopic data for small  $\tau$ . For these one would need to increase  $N$  and wait much longer to obtain satisfying graphs.

[1] C. Cohen-Tannoudji, B. Diu, and F. Laloe, *Quantenmechanik, Band 1* (de Gruyter, Berlin, 2009).  
[2] V. B. Braginsky and F. Y. Khalili, *Quantum Measurement* (Cambridge University Press, Cambridge, 1992).  
[3] Y. Shikano, K. Chisaki, E. Segawa, and N. Konno, *Phys. Rev. A* **81**, 062129 (2010).  
[4] M. Gönülol, E. Aydın, Y. Shikano, and Ö. E. Müstecaplıoğlu, *New J. Phys.* **13**, 033037 (2011).  
[5] J. Yi, P. Talkner, and G.-L. Ingold, *Phys. Rev. A* **84**, 032121 (2011).  
[6] S. Gurvitz, *Fortschr. Phys.* **65**, 1600065 (2017).

[7] B. Mukherjee, K. Sengupta, and S. N. Majumdar, *Phys. Rev. B* **98**, 104309 (2018).  
[8] D. C. Rose, H. Touchette, I. Lesanovsky, and J. P. Garrahan, *Phys. Rev. E* **98**, 022129 (2018).  
[9] Y. Ashida, K. Saito, and M. Ueda, *Phys. Rev. Lett.* **121**, 170402 (2018).  
[10] E. Bach, S. Coppersmith, M. P. Goldschen, R. Joynt, and J. Watrous, *J. Comput. Syst. Sci.* **69**, 562 (2004).  
[11] H. Krovi and T. A. Brun, *Phys. Rev. A* **73**, 032341 (2006).  
[12] H. Krovi and T. A. Brun, *Phys. Rev. A* **74**, 042334 (2006).  
[13] H. Krovi and T. A. Brun, *Phys. Rev. A* **75**, 062332 (2007).

- [14] M. Varbanov, H. Krovi, and T. A. Brun, *Phys. Rev. A* **78**, 022324 (2008).
- [15] F. A. Grünbaum, L. Velázquez, A. H. Werner, and R. F. Werner, *Commun. Math. Phys.* **320**, 543 (2013).
- [16] J. Bourgain, F. A. Grünbaum, L. Velázquez, and J. Wilkening, *Commun. Math. Phys.* **329**, 1031 (2014).
- [17] M. Štefaniák, I. Jex, and T. Kiss, *Phys. Rev. Lett.* **100**, 020501 (2008).
- [18] S. Dhar, S. Dasgupta, and A. Dhar, *J. Phys. A: Math. Theor.* **48**, 115304 (2015).
- [19] S. Dhar, S. Dasgupta, A. Dhar, and D. Sen, *Phys. Rev. A* **91**, 062115 (2015).
- [20] S. Lahiri and A. Dhar, *Phys. Rev. A* **99**, 012101 (2019).
- [21] P. Sinkovicz, Z. Kurucz, T. Kiss, and J. K. Asbóth, *Phys. Rev. A* **91**, 042108 (2015).
- [22] P. Sinkovicz, T. Kiss, and J. K. Asbóth, *Phys. Rev. A* **93**, 050101(R) (2016).
- [23] H. Friedman, D. A. Kessler, and E. Barkai, *J. Phys. A: Math. Theor.* **50**, 04LT01 (2017).
- [24] H. Friedman, D. A. Kessler, and E. Barkai, *Phys. Rev. E* **95**, 032141 (2017).
- [25] F. Thiel, E. Barkai, and D. A. Kessler, *Phys. Rev. Lett.* **120**, 040502 (2018).
- [26] F. Thiel, D. A. Kessler, and E. Barkai, *Phys. Rev. A* **97**, 062105 (2018).
- [27] F. Thiel, I. Mualem, D. A. Kessler, and E. Barkai, *Phys. Rev. Research* **2**, 023392 (2020).
- [28] F. Thiel, I. Mualem, D. Meidan, E. Barkai, and D. A. Kessler, [arXiv:1906.08112](https://arxiv.org/abs/1906.08112).
- [29] F. Thiel, D. A. Kessler, and E. Barkai, [arXiv:1912.08649](https://arxiv.org/abs/1912.08649).
- [30] G. R. Allcock, *Ann. Phys. (NY)* **53**, 253 (1969).
- [31] G. R. Allcock, *Ann. Phys. (NY)* **53**, 286 (1969).
- [32] G. R. Allcock, *Ann. Phys. (NY)* **53**, 311 (1969).
- [33] J. A. Damborenea, I. L. Egusquiza, G. C. Hegerfeldt, and J. G. Muga, *Phys. Rev. A* **66**, 052104 (2002).
- [34] E. A. Galapon, F. Delgado, J. G. Muga, and I. Egusquiza, *Phys. Rev. A* **72**, 042107 (2005).
- [35] J. Echanobe, A. del Campo, and J. G. Muga, *Phys. Rev. A* **77**, 032112 (2008).
- [36] J. G. Muga, J. Echanobe, A. del Campo, and I. Lizuain, *J. Phys. B* **41**, 175501 (2008).
- [37] A. Ruschhaupt, J. G. Muga, and G. C. Hegerfeldt, Detector Models for the Quantum Time of Arrival, in *Time in Quantum Mechanics - Vol. 2*, edited by G. Muga, A. Ruschhaupt, and A. del Campo, Lecture Notes in Physics Vol. 789 (Springer, Berlin, Heidelberg, 2009).
- [38] D. L. Sombillo and E. A. Galapon, *Phys. Rev. A* **90**, 032115 (2014).
- [39] D. L. B. Sombillo and E. A. Galapon, *Ann. Phys. (NY)* **364**, 261 (2016).
- [40] S. Redner, *A Guide to First-Passage Processes*, 1st ed. (Cambridge University Press, Cambridge, 2007).
- [41] O. Bénichou, C. Loverdo, M. Moreau, and R. Voituriez, *Rev. Mod. Phys.* **83**, 81 (2011).
- [42] O. Bénichou, T. Guérin, and R. Voituriez, *J. Phys. A: Math. Theor.* **48**, 163001 (2015).
- [43] D. Hartich and A. Godec, *J. Stat. Mech.* (2019) 024002.
- [44] D. Hartich and A. Godec, *J. Phys. A: Math. Theor.* **52**, 244001 (2019).
- [45] L. K. Grover, *Phys. Rev. Lett.* **79**, 325 (1997).
- [46] S. Aaronson and A. Ambainis, in *Proceedings of the 44th Annual IEEE Symposium on Foundations of Computer Science, Cambridge, 2003* (IEEE, Piscataway, 2003), pp. 200–209.
- [47] A. M. Childs and J. Goldstone, *Phys. Rev. A* **70**, 022314 (2004).
- [48] F. Magniez, A. Nayak, J. Roland, and M. Santha, *SIAM J. Comput.* **40**, 142 (2011).
- [49] S. Chakraborty, L. Novo, A. Ambainis, and Y. Omar, *Phys. Rev. Lett.* **116**, 100501 (2016).
- [50] S. Li and S. Boettcher, *Phys. Rev. A* **95**, 032301 (2017).
- [51] A. Kay, *Int. J. Quantum Inf.* **08**, 641 (2010).
- [52] B. Misra and E. C. G. Sudarshan, *J. Math. Phys.* **18**, 756 (1977).
- [53] W. M. Itano, D. J. Heinzen, J. J. Bollinger, and D. J. Wineland, *Phys. Rev. A* **41**, 2295 (1990).
- [54] T. J. Elliott and V. Vedral, *Phys. Rev. A* **94**, 012118 (2016).
- [55] F. Schäfer, I. Herrera, S. Cherukattil, C. Lovecchio, F. S. Cataliotti, F. Caruso, and A. Smerzi, *Nat. Commun.* **5**, 3194 (2014).
- [56] M. M. Müller, S. Gherardini, and F. Caruso, *Ann. Phys. (Berlin)* **529**, 1600206 (2017).
- [57] H.-V. Do, C. Lovecchio, I. Mastroserio, N. Fabbri, F. S. Cataliotti, S. Gherardini, M. M. Müller, N. D. Pozza, and F. Caruso, *New J. Phys.* **21**, 113056 (2019).
- [58] R. M. Pearlstein, *J. Chem. Phys.* **56**, 2431 (1972).
- [59] P. L. Krapivsky, J. M. Luck, and K. Mallick, *J. Stat. Phys.* **154**, 1430 (2014).
- [60] F. Delgado, J. G. Muga, and G. García-Calderón, *Phys. Rev. A* **74**, 062102 (2006).
- [61] L. S. Schulman, *Phys. Rev. A* **57**, 1509 (1998).
- [62] N. Moiseyev, *Non-Hermitian Quantum Mechanics* (Cambridge University Press, Cambridge, 2011).
- [63] Y. K. Ho, *Phys. Rep.* **99**, 1 (1983).
- [64] P. Meystre and E. M. Wright, *Phys. Rev. A* **37**, 2524 (1988).
- [65] J. Dalibard, Y. Castin, and K. Mølmer, *Phys. Rev. Lett.* **68**, 580 (1992).
- [66] N. Gisin and I. C. Percival, *J. Phys. A: Math. Gen.* **25**, 5677 (1992).
- [67] A. Buchleitner, B. Grémaud, and D. Delande, *J. Phys. B* **27**, 2663 (1994).
- [68] M. B. Plenio and P. L. Knight, *Rev. Mod. Phys.* **70**, 101 (1998).
- [69] T. A. Brun, *Am. J. Phys.* **70**, 719 (2002).
- [70] F. Caruso, A. W. Chin, A. Datta, S. F. Huelga, and M. B. Plenio, *J. Chem. Phys.* **131**, 105106 (2009).
- [71] E. Agliari, O. Mülken, and A. Blumen, *Int. J. Bifurcat. Chaos* **20**, 271 (2010).
- [72] O. Mülken and A. Blumen, *Phys. Rep.* **502**, 37 (2011).
- [73] G. G. Giusteri, F. Mattiotti, and G. L. Celardo, *Phys. Rev. B* **91**, 094301 (2015).
- [74] L. Novo, S. Chakraborty, M. Mohseni, H. Neven, and Y. Omar, *Sci. Rep.* **5**, 13304 (2015).
- [75] Y. Xu, S.-T. Wang, and L.-M. Duan, *Phys. Rev. Lett.* **118**, 045701 (2017).
- [76] E. Rivet, A. Brandstötter, K. G. Makris, H. Lissek, S. Rotter, and R. Fleury, *Nat. Phys.* **14**, 942 (2018).
- [77] L. Xiao, K. Wang, X. Zhan, Z. Bian, K. Kawabata, M. Ueda, W. Yi, and P. Xue, *Phys. Rev. Lett.* **123**, 230401 (2019).

- [78] S. Lapp, J. Ang'ong'a, F. A. An, and B. Gadway, *New J. Phys.* **21**, 045006 (2019).
- [79] J. Li, A. K. Harter, J. Liu, L. de Melo, Y. N. Joglekar, and L. Luo, *Nat. Commun.* **10**, 855 (2019).
- [80] A. G. Redfield, *IBM J. Res. Dev.* **1**, 19 (1957).
- [81] P. Facchi and S. Pascazio, *J. Phys. A: Math. Theor.* **41**, 493001 (2008).
- [82] R. Yin, K. Ziegler, F. Thiel, and E. Barkai, *Phys. Rev. Res.* **1**, 033086 (2019).
- [83] Q. Liu, R. Yin, K. Ziegler, and E. Barkai, [arXiv:2001.00231](https://arxiv.org/abs/2001.00231) [Phys. Rev. Research (to be published)].
- [84] M. S. Fadali and A. Visioli, *Digital Control Engineering, Analysis and Design* (Academic, Amsterdam, 2013).
- [85] N. Moiseyev, *Phys. Rep.* **302**, 212 (1998).
- [86] J. Muga, J. Palao, B. Navarro, and I. Egusquiza, *Phys. Rep.* **395**, 357 (2004).
- [87] H. Feshbach, *Ann. Phys. (NY)* **5**, 357 (1958).
- [88] M. S. Rudner and L. S. Levitov, *Phys. Rev. Lett.* **102**, 065703 (2009).
- [89] T. Nitsche, S. Barkhofen, R. Kruse, L. Sansoni, M. Štefaňák, A. Gábris, V. Potoček, T. Kiss, I. Jex, and C. Silberhorn, *Sci. Adv.* **4**, eaar6444 (2018).
- [90] I. S. Gradshteyn and I. M. Ryzhik, in *Table of Integrals, Series and Products*, 7th ed., edited by A. Jeffrey and D. Zwillinger (Academic, Amsterdam, 2007).
- [91] A. P. Prudnikov, Y. A. Brychkov, and O. I. Marichev, *Integrals and Series: Inverse Laplace Transforms* (Gordon and Breach, New York, 1992), Vol. 5.